UPPSALA
UNIVERSITET

Digital Comprehensive Summaries of Uppsala Dissertations from the Faculty of Science and Technology 554

Modelling and Degradation Characteristics of Thin-film CIGS Solar Cells

ULF MALM

ACTA
UNIVERSITATIS
UPSALIENSIS
UPPSALA
2008

ISSN 1651-6214
ISBN 978-91-554-7287-0
urn:nbn:se:uu:diva-9291

Dissertation presented at Uppsala University to be publicly examined in Häggsalen, Ångströmlaboratoriet, Lägerhyddsvägen 1, Uppsala, Friday, October 17, 2008 at 09:30 for the degree of Doctor of Philosophy. The examination will be conducted in English.

Abstract
Malm, U. 2008. Modelling and Degradation Characteristics of Thin-film CIGS Solar Cells. Acta Universitatis Upsaliensis. *Digital Comprehensive Summaries of Uppsala Dissertations from the Faculty of Science and Technology* 554. 81 pp. Uppsala. ISBN 978-91-554-7287-0.

Thin-film solar cells based around the absorber material $CuIn_{1-x}Ga_xSe_2$ (CIGS) are studied with respect to their stability characteristics, and different ways of modelling device operation are investigated. Two ways of modelling spatial inhomogeneities are detailed, one fully numerical and one hybrid model. In the numerical model, thin-film solar cells with randomized parameter variations are simulated showing how the voltage decreases with increasing material inhomogeneities.

With the hybrid model, an analytical model for the p-n junction action is used as a boundary condition to a numerical model of the steady state electrical conduction in the front contact layers. This also allows for input of inhomogeneous material parameters, but on a macroscopic scale. The simpler approach, compared to the numerical model, enables simulations of complete cells. Effects of material inhomogeneities, shunt defects and grid geometry are simulated.

The stability of CIGS solar cells with varying absorber thickness, varying buffer layer material and CIGS from two different deposition systems are subjected to damp heat treatment. During this accelerated ageing test the cells are monitored using characterization methods including J-V, QE, C-V and $J(V)_T$. The degradation studies show that the typical V_{OC} decrease experienced by CIGS cells subjected to damp heat is most likely an effect in the bulk of the absorber material.

When cells encapsulated with EVA are subjected to the same damp heat treatment, the effect on the voltage is considerably reduced. In this situation the EVA is saturated with moisture, representing a worst case scenario for a module in operation. Consequently, real-life modules will not suffer extensively from the V_{OC} degradation effect, common in unprotected CIGS devices.

Keywords: solar cells, thin-film, chalcogenide, stability, characterization, modelling, simulations, finite element method, CIGS, photovoltaic module

Ulf Malm, Department of Engineering Sciences, Solid State Electronics, Box 534, Uppsala University, SE-75121 Uppsala, Sweden

ISSN 1651-6214
ISBN 978-91-554-7287-0
urn:nbn:se:uu:diva-9291 (http://urn.kb.se/resolve?urn=urn:nbn:se:uu:diva-9291)

For my Honey Bee
and the Mandarin

List of Papers

This thesis is based on the following papers, which are referred to in the text by their Roman numerals.

I Malm, U. and Edoff, M. 2-D Device Modelling and Finite Element Simulations for Thin-film Solar Cells,
Submitted to *Solar Energy Materials and Solar Cells*

II Malm, U. and Edoff, M. Influence from front contact sheet resistance on extracted diode parameters in CIGS solar cells, *Progress in Photovoltaics: Research and Applications*, 2008, 16, 113–121

III Malm, U. and Edoff, M. Simulating Material Inhomogeneities and Defects in CIGS Thin-film Solar Cells
Submitted to *Progress in Photovoltaics: Research and Applications*

IV Malm, U., Edoff, M. and Stolt, L. The Stability in Damp Heat Conditions of Thin-film CIGS Solar Cells With Different Absorber Thickness, in: *Proceedings of the 19th European Photovoltaic Solar Energy Conference*, 2004, 1890–1893

V Malm, U. and Stolt, L. Long term stability in Cu(In,Ga)Se_2 solar cells with different buffer materials, in: *Proceedings of the 20th European Photovoltaic Solar Energy Conference*, 2005, 1930–1933

VI Malm, U., Carlsson, T. and Edoff, M. Stability in Cu(In,Ga)Se_2 Solar Cells with EVA Encapsulation in Varying Damp Heat Conditions, in: *Proceedings of the 21st European Photovoltaic Solar Energy Conference*, 2006, 1990–1993

VII Malm, U., Malmström, J., Platzer-Björkman, C. and Stolt, L. Determination of dominant recombination paths in Cu(In,Ga)Se_2 thin-film solar cells with ALD-ZnO buffer layers *Thin Solid Films*, 2005, 480–481, 208–212

List of Additional Papers

The author has been involved in the following publications that are not included in this thesis.

i Carlsson, T., Konttinen, P., Malm, U. and Lund, P. Absorption and desorption of water in glass/ethylene-vinyl-acetate/glass laminates *Polymer Testing*, 2006, 25, 615-622

ii Edoff, M., Malmberg, L., Malm, U. and Stolt, L. Influence of CBD-Deposited CdS on the Carrier Collection in CIGS-Based Solar Cells, in: *Conference Record of the 2006 IEEE 4th World Conference on Photovoltaic Energy Conversion*, 2006, 1, 396-399

Contents

List of Tables

List of Figures

List of symbols

Symbol	Explanation	Unit
J	Current density	[mA/cm^2]
V	Bias voltage	[V]
C	Capacitance	[F/cm^2]
J_0	Saturation current density	[mA/cm^2]
J_{00}	Saturation current prefactor	[mA/cm^2]
A	Diode ideality factor	[-]
R_s	Series resistance	[kΩcm^2]
G_{sh}	Shunt conductance	[mS/cm^2]
J_L	Photo current density	[mA/cm^2]
V_{OC}	Open circuit voltage	[V]
J_{SC}	Short circuit current density	[mA/cm^2]
FF	Fill factor	[%]
η	Conversion efficiency	[%]
E_F	Fermi level	[eV]
E_{Fp}, E_{Fn}	Hole and electron Fermi levels	[eV]
E_C	Conduction band minimum	[eV]
E_V	Valence band maximum	[eV]
E_g	Band gap energy	[eV]
ΔE_C	Conduction band offset	[eV]
E_a	Recombination activation energy	[eV]
Φ_b^p	Hole barrier at absorber/buffer interface	[eV]
n_i	Intrinsic carrier concentration	[cm^{-3}]
E_i	Intrinsic Fermi level	[eV]
N_A	Acceptor concentration (ionized)	[cm^{-3}]
N_D	Donor concentration (ionized)	[cm^{-3}]
n	Electron concentration	[cm^{-3}]
p	Hole concentration	[cm^{-3}]
n_0	Equilibrium electron concentration	[cm^{-3}]
p_0	Equilibrium hole concentration	[cm^{-3}]
G	Generation rate	[cm^{-2}s^{-1}]
R	Recombination rate	[cm^{-2}s^{-1}]
Ψ	Electric potential	[V]
q	Elemental charge	[J]
T	Temperature	[K]

μ_e	Electron mobility	[cm^2/Vs]
μ_p	Hole mobility	[cm^2/Vs]
D_e	Electron diffusion constant	[cm^2/s]
D_p	Hole diffusion constant	[cm^2/s]
S_n	Electron recombination velocity	[cm/s]
S_p	Hole recombination velocity	[cm/s]
J_n	Electron current density	[mA/cm^2]
J_p	Hole current density	[mA/cm^2]
ε_0	Permittivity of vacuum	[As/Vcm]
ε_r	Relative permittivity	[-]
ε_s	Semiconductor permittivity	[As/Vcm]
V_{bi}	Built in voltage	[V]
CIGS	$Cu(In,Ga)Se_2$	
CIS	$CuInSe_2$	
CGS	$CuGaSe_2$	
ZAO	Aluminium doped ZnO	
TCO	Transparent conductive oxide	
EVA	Ethylene-vinyl acetate	
SLG	Soda lime glass	
QE	Quantum efficiency	
J-V	Current–voltage characteristics	
C-V	Capacitance–voltage characteristics	
$J(V)_T$	Temperature dependent *J-V*	
ODM	One diode model	
D.H.	Damp heat	
PVD	Physical vapour deposition	
UV	Ultraviolet	
IR	Infrared	
PV	Photovoltaic	

1. Introduction

All energy on Earth, barring geothermic and nuclear energy, ultimately comes from the sun. The resource of solar energy is vast compared to the energy needed today - as an example 17 times the total primary energy consumption could be supplied by solar cells in the desert areas of the World [49]. Although these numbers are hypothetical they do indicate the enormity of the resource available from the Sun. The key question is how we harness this energy and shape it into the most useful form.

1.1 A Short History of Solar Energy

Solar energy useful to man in its simplest form is when you go outside and feel the warming rays of the sun or when you hang your clothes out to dry in a gentle breeze. This way of using solar energy is as old as humanity, but nonetheless still extremely important to us. Over the past hundred years, the technological advances have brought with it a need for different forms of energy. The direct heat from the sun will not power your mobile phone.

There are lots of ways of converting solar energy into, e.g., electric energy. From the industrial revolution through the early industrial age, coal-fired power dominated, but was subsequently surpassed by oil-fired power from the mid 20th century [53]. Both these energy sources are solar energy by proxy (although there are scientists questioning the biogenic nature of hydrocarbons, e.g. [60]). The solar energy was once stored in biomass, which subsequently was transformed to various fossil fuels over time. As most people realize today, fossil fuel resources are limited. This has turned the public eye towards biofuels.

Biomass harness the energy from the sun through the photosynthesis process in plants, and has been used as fuel long before the fossil fuels were available. One example is wood burned for heat or cooking, or crops grown for food. Today it is becoming increasingly popular as a source of electricity or as fuels for our cars. Other forms of indirect solar energy that are used today are hydro, wind and wave power.

1.2 Modern Solar Energy

One of the key issues for humanity in the future will be energy. Access to and control over energy resources will be evermore crucial as inequalities in the

World start to even out and the economies in developing countries grow at a fast pace. The energy usage in the World will increase.

In order to meet this rising demand, new energy generation technologies must be used together with the more conventional forms of renewable energy mentioned previously.

This is where solar cells come in. They offer an efficient use of the energy from the sun. The overall conversion efficiency of a PV systems today is in the range of 10 %, which is high compared to other routes of utilizing the solar energy. As an example, a recent study showed a net energy yield of 60 GJ/(ha·y) for cellulosic ethanol made from switchgrass grown in the U.S. midwest [69]. A PV system with horizontal orientation would in the same region yield approximately 6 000 GJ/(ha·y). This example is calculated with a PV array efficiency of 12 %, a performance ratio of 80 % and an annual insolation of 1 640 kWh/m^2. Other benefits are that once erected, a photovoltaic energy system can operate with very little maintenance, there is little risk for the surroundings and the aesthetics are rarely a problem.

There are, of course, drawbacks of PV technology such as the fact that storage is needed for when the sun does not shine. However, the major obstacle for a large scale deployment today is the price. Factoring in a number of different variables, such as amount of sunshine, interest rates, system lifetime and alternative energy costs, electricity from PV is from two to five times as expensive as the electricity from conventional sources. This means that today the PV market needs to be subsidized in order to sustain its growth. In the long run, the main goal of the PV comunity is to aim for grid-parity, i.e. when the price of PV electricity matches that of electric energy bought from the grid.

1.3 Developing Solar Cells For the Future

Ultimately, in order to reach grid-parity, the price for electricity from a solar cell system must come down in relation to the price of electricity generated by other means. This can be accomplished in several ways, most prominently by reducing costs in production, extending lifetime of systems or penalizing alternatives.

One way of decreasing costs is to use thin-film technology, which allows for rational large scale production. There are several technology systems in this category, and one of them, based around the absorber material Cu(In,Ga)Se_2 also known as CIGS, is the main concern of this thesis. While not as mature as the dominant Si wafer technology, thin-film technologies promise cost-reductions in large scale production with monolithical interconnection and low material usage. In order to realize these promises, the material system used in these devices must be thoroughly understood. One way of increasing the understanding of device operation is through modelling and simulations.

Modelling is widely used in development of electronic devices, e.g., thin-film solar cells. It has been applied to various solar cell problems [84, 82, 72, 46, 55, 12, 64, 74, 26], modelling the complete cell operation or parts of

it. In addition to modelling of the devices themselves, there are also process simulations that are used to design and study the deposition processes. Most input material parameters come from measurements, but in the case of CIGS devices there are several parameters that are difficult to measure, and the measurements results are sometimes difficult to analyse. Modelling for increased understanding of the influence of material properties on performance is studied in this thesis.

One particular field that is not very well understood in the case of CIGS solar cells is that of long term stability and degradation. The stability of CIGS-based devices have been studied by several authors [31, 48, 52, 65, 76, 92], and the general picture can be summarized as being disparate. In some respects this type of device seems to be stable over time, but on the other hand they often exhibit a sensitivity to moisture that may be a problem in long term use. The stability of CIGS solar cells in damp heat, with variations in absorber thickness and buffer layer material is investigated in this work. The effects of damp heat on cells encapsulated in EVA is also studied.

In summary, this thesis deals with the complex issues of modelling, characterizing, and ultimately, understanding of effects of CIGS-based solar cell devices. Especially in connection with empirical observations on stability of the devices.

2. Solar Cells

Solar cells, in a general sense electronic devices that generate electricity when illuminated, operate through the photovoltaic effect discovered by Alexandre-Edmond Becquerel in 1839 [6]. Hence the collective noun *photovoltaics*, or in short PV, which denotes photovoltaic power systems, components, or the solar cell industry as whole. In this thesis the concept of photovoltaics will be used in a broad sense concerning systems and industry, while the term solar cell will be used when devices are concerned.

2.1 The Photovoltaic Effect

The essence of the photovoltaic effect can be derived from the origin of its name, being made up from *photo* (from the Greek word phos = light) and *voltaic* (electrical, derived from the name of Italian physicist Alessandro Volta). Hence, the photovoltaic effect is about electricity from light.

In the original experiment by Becquerel [6], the photovoltaic effect was observed at electrodes immersed in a liquid electrolyte, but today most solar cells are solid state semiconductor p-n junction devices. However, the effect is the same, with photons exciting carriers that are extracted as electric energy that can be put to use in an external load. In this text, only solid state semiconductor solar cells will be treated.

When a solar cell is illuminated, typically with solar irradiation, photons enter the structure and excite electrons from the valence band to the conduction band, creating electron-hole pairs. In the p-type part of the device electrons diffuse and are driven by the electric field towards the n-type part of the device. The opposite is true for generation in the n-type part of the device, with holes diffusing and being driven towards the p-type side. This creates a charge separation, which leads to a voltage difference between the two sides, which can drive current through an external load and the charge carriers are circulated through the system. Figure 2.1 illustrates this operating principle.

The power delivered to the external load is chiefly governed by the irradiation that reaches the cell and the load itself. With a low impedance load, the current will be close to that delivered into a short circuit connection (J_{SC}) while the voltage is low. For a high impedance load the converse is true, with a voltage close to the open circuit voltage (V_{OC}) and a low current.

During normal operation the current is defined as negative. This is merely a convention that stems from the current being defined as positive in the forward direction of the *p-n* junction, which means that power is delivered to the

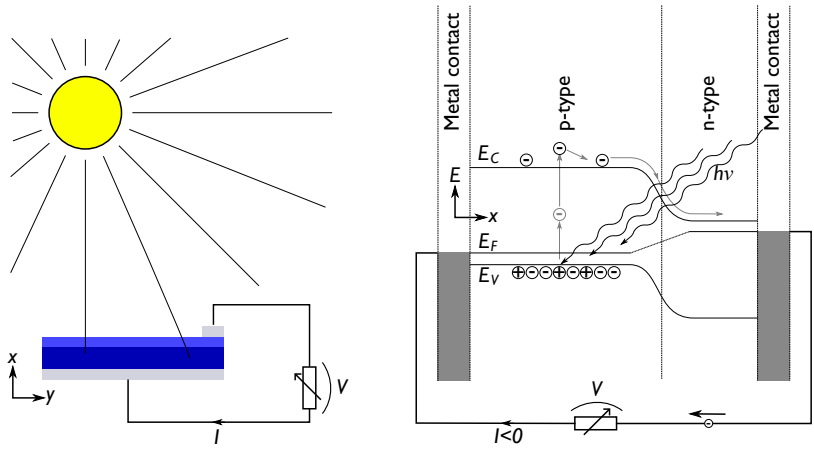

Figure 2.1: A schematic showing the basic operation of solar cells. The device is illuminated with, e.g., solar irradiation. The radiation excites carriers across the band gap of the absorber material, and charge is separated by the *p-n* junction.

external load circuit in the fourth quadrant of a current-voltage plot measured under illumination. This kind of plot, a *J-V* curve, is used very often in solar cell research and is described more extensively in Section 4.1.

2.2 Solar Cell Research

With the photovoltaic effect discovered in the mid 19th century, no practically usable photovoltaic cell was created until more than 100 years later, in the beginning of the semiconductor era. It was, like several other semiconductor devices, first realized in Bell labs in the mid 20th century. More specifically, this was a 6 % efficient silicon solar cell made by Chapin, Fuller and Pearson in 1954 [17, 28].

2.2.1 A Developing Field of Research

Subsequently the photovoltaic technology was adopted by the space industry, where it was used as a source of energy for communication satellites. The space race in the 50-ies and 60-ies provided the main development incentives for better solar cells and saw the introduction of GaAs cells [3], which provide higher efficiency but at a cost. This technology still heavily dominates the space cell market.

Another reason for solar cell research emerged with the oil crisis in the early 70-ies and efforts were renewed, not just in solar cell research but in all fields of energy technology. This is illustrated in Figure 2.2, where the number of articles indexed in Inspec with the term “photovoltaics” in the controlled vocabulary in relation to total number of articles is shown.

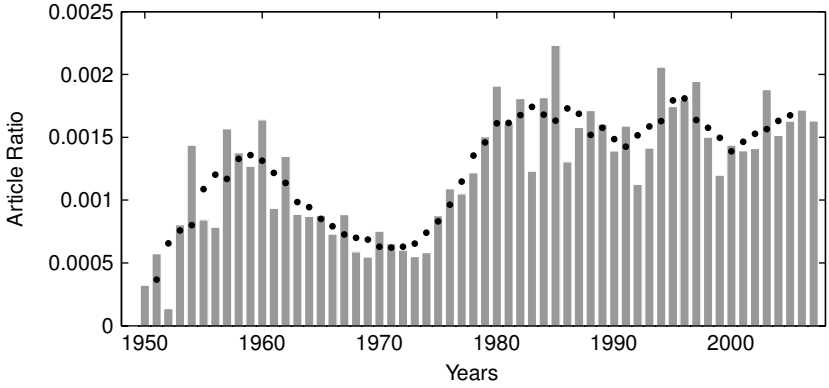

Figure 2.2: The number of articles indexed in Inspec with the term "photovoltaics" in the controlled vocabulary divided by the total number of articles from 1949 to 2007 (bars). The circles denote the moving average over five years in order to more clearly show the trends.

2.2.2 Solar Cell Research Today

90 % of all solar cell modules installed today are wafer-based Si ones [79]. This dominance of Si is also apparent in the amount of research going on, albeit not as large as in the installed power. Often, the wafer-based Si technology is referred to as first generation technology, while different kinds of thin-film ones are referred to as second generation. The third generation is a little more difficult to categorize, but most often it denotes a group of technologies that are yet to be realized on a larger scale, but with promising cost–efficiency characteristics.

With the wafer-based Si technology being reasonably mature, most of the research is directed towards production. The price reductions in this technology has been steady at approximately 20 % per doubling of the shipped rated peak power during the past ten to twenty years [33]. With different technologies belonging to the second generation technology, e.g. thin-film Si, CdTe and CIGS, nearing in on large scale production the potentials for cost reductions increase. With the increasing maturity of the CIGS technology, and the introduction of CIGS modules to the photovoltaics market on a larger scale, the development of manufacturing technology is mostly carried out by companies, while more basic research for future improvements and fundamental understanding is generally conducted by universities.

3. CIGS Thin-film Technology

$CuIn_{1-x}Ga_xSe_2$-based thin-film solar cells (often called "CIGS cells") are multi-layer thin-film components, most often deposited on glass substrates. The thin-film deposition, with monolithic interconnection of individual cells, on relatively cheap substrates is the great advantage of thin-film technologies compared to a wafer-based one where individual cells need to be soldered together into strings and laid out into a module. In this text the term CIGS will be used to denote material with $x \approx 0.3$, but also in reference to the whole material system (from CIS to CGS).

3.1 Cell Structure

CIGS solar cells are most often formed on rigid substrates of soda lime glass (SLG), but essentially any substrate could be feasible. The reasons for choosing SLG are that it is electrically insulating, comparatively cheap, temperature stable and with a smooth surface. Alternative substrate materials used are, e.g., Ti and polyimide foils. With an electrically conducting substrate there has to be an insulating barrier if the device is to contain monolithically interconnected cells.

On the substrate, the back contact is deposited using physical vapour deposition (PVD), most often sputtering. Mo is the contact material of choice in the CIGS community, due to its inertness in subsequent deposition steps and its ability to create an ohmic contact to the CIGS material in the presence of $MoSe_2$ [73, 88]. For modules, this layer is patterned in order to separate one cell from the next (cf. Section 3.2).

On top of this contact layer, the CIGS absorber material is deposited. CIGS can be synthesized in several ways, PVD being the most important one today. Most of the companies that produce CIGS solar cell modules for the market use this kind of absorber deposition technology, but there are several companies and research institutions working with low-cost solutions, like printing of nanoparticle compounds or electrodeposition (see e.g. [39, 85]).

The PVD methods for depositing CIGS can be divided into several groups, as well. The two most important ones are sequential elemental sputtering followed by selenization, and co-evaporation. In the method with elemental sputtering, layers of Cu, In and Ga are sputtered onto the substrate. Subsequently the metal precursors are annealed in an Se atmosphere, so that they are selenized and form a layer of $Cu(In,Ga)Se_2$ [7].

In the co-evaporation method, used for all samples in the experiments of this thesis, the three metals are evaporated from elemental sources, in an atmosphere of selenium abundance. The material composition can be controlled through parameters like the rates of the sources, their position, the geometry of the deposition chamber and the movement of substrates. In a production type deposition system, an in-line process is typically used with stationary sources and the substrates moving past them (see e.g. [59]).

On top of the CIGS absorber layer, a buffer layer is deposited, most often using a wet chemical method called Chemical Bath Deposition (CBD). The role of the buffer layer has been debated, but its main roles are to passivate the absorber surface and to provide a suitable partnering material to make up the hetero junction, combined with the following ZnO/ZAO double layer. Attempts at using ZnO directly on the CIGS have failed due to excessive recombination at the interface between the layers (see Paper VII). The most common material today is CdS, but several alternatives, like (Zn,Mg)O and Zn(O,S) deposited using both wet chemical and vacuum methods, are researched since they may provide spectral response benefits and are non-toxic as opposed to the Cd used in CdS (see [83, 58]).

The buffer layer is followed by a thin layer of highly resistive ZnO, which has multiple benefits. It may protect the surface from damage in subsequent process steps, but its most important use is that it evens out the potential, so that small shunt conductances are isolated and rendered practically harmless.

The solar cell devices are finished off with the front contact layer consisting of a transparent conducting oxide (TCO). In the cells used in this study, this TCO consists of heavily Al-doped ZnO (ZAO). This layer plays a very important role in the hybrid modelling described in Section 5.4. The CIGS structure, with its most common configuration is illustrated in Figure 3.1a

3.2 Module Interconnection

One of the main advantages of thin-film solar cell modules, as compared to wafer-based ones, is that in thin-film modules the cells can be interconnected monolithically. This means that the series connection is performed already in the manufacturing process, without the need to solder individual cells into strings.

This series interconnection is accomplished by patterning the thin-film layers during the in-line processing. In order to make a series connection of cells, three patterning steps are typically required. The first one separates the back contact material (Mo) for the different cells, simply making trenches in the metal layer (see P1 in Figure 3.1b). This patterning is most often accomplished through laser scribing.

Subsequently, the absorber and buffer layers are deposited as well as the highly resistive ZnO layer. These layers are then patterned using a mechanical scriber, making a trench (P2) that does not penetrate the Mo layer. When the conducting window material (ZAO) is deposited it forms an essentially

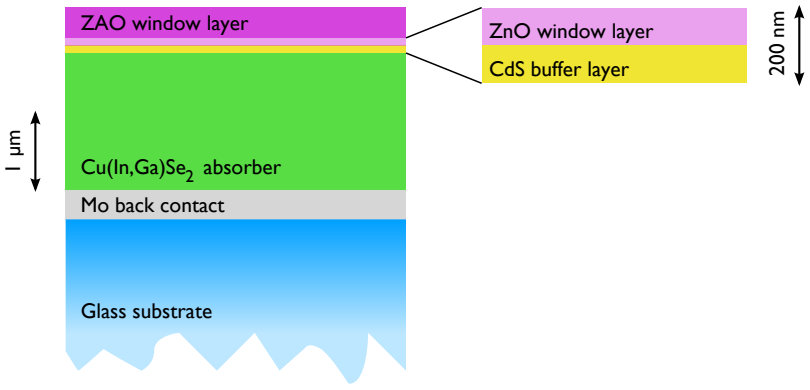

(a) The most common CIGS cell configuration.

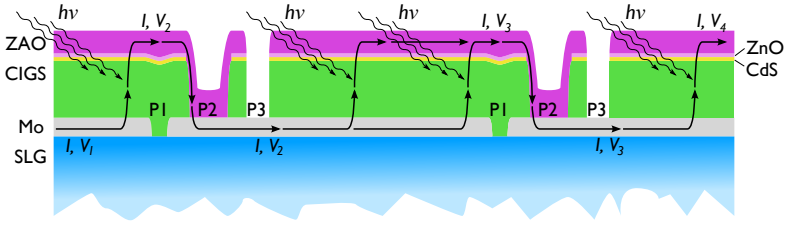

(b) Interconnect structure used in CIGS thin-film solar cell modules.

Figure 3.1: Schematic drawings of the cell structure (a) and the module interconnect structure (b) most often used in CIGS devices.

ohmic contact to the Mo back contact of the next cell in the P2 trench. This P2 trench can also be made before the ZnO layer, or by modifying the CIGS to a conducting material through laser exposure [90]. To finish off the series interconnection, a third scribe (P3) is made through all layers but the Mo back contact, so that the front contacts of adjacent cells are separated from each other. The current is constant through the cells in series, while the voltage increases for each cell so that $V_1 < V_2 < V_3$.

4. Characterization techniques

The main themes in this work are intimately connected with electrical characterization techniques for thin-film solar cells. These different techniques are used as a feed back to process development and to gain deeper understanding of the operation of the cell. In the chapter on modelling (5) the result of the simulations are in the form of measurement data, which can be compared to that of actual measurements. Other measurement quantities are used as input to simulations, or in order to validate simulation results. In the chapter on stability studies (6), the measurement techniques are used to monitor the degradation of cells.

4.1 *J-V*

The most important characterization technique for solar cells is the current-voltage (*I-V*) characterization, or more often current density versus voltage (*J-V*). This is used as a routine measurement method applied to nearly all cells made in a manufacturing or laboratory environment. It is acquired using a so called solar simulator, schematically illustrated in Figure 4.1a. This measurement set-up typically consists of a light source (I), sample stage with temperature control (II), an external source measure unit (SMU) or a variable load (III) and a computer for data acquisition (IV). These *J-V* measurements are almost always made at a reference temperature of 25 °C and with illumination that complies with a reference spectrum, like the AM1.5G [1].

The *J-V* measurements most importantly result in the four solar cell parameters often used to characterize the device, J_{SC}, V_{OC}, FF and η. These constitute basic tools for evaluation of cell performance, with the short circuit current, J_{SC}, indicating the absorption of photons and collection of carriers. The open circuit voltage, V_{OC}, is governed by the band gap of the absorber, but also by the degree of recombination in the cell. The J_{SC} and the V_{OC} parameters are simply the current and voltage at the two points where the *J-V* curve intersects the current and voltage axes, respectively. These points are marked with red circles on the curve in Figure 4.1.

The fill factor, FF, is the ratio of the maximum output power to the product of J_{SC} and V_{OC}. Thus, it is a measure of the "squareness" of the *J-V* curve in the fourth quadrant. The maximum power point is marked with a red circle in Figure 4.1. The efficiency, η, is the ratio of maximum output power to input power.

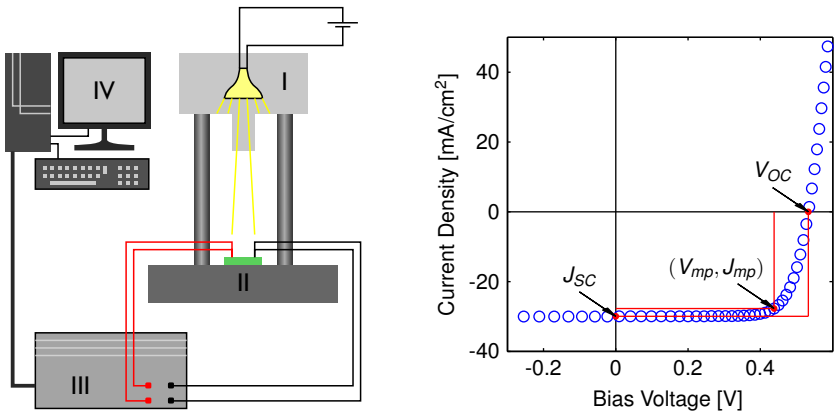

(a) J-V set-up *(b) J-V* curve example

Figure 4.1: A schematic drawing of a typical *J-V* measurement set up (solar simulator) and a typical illuminated *J-V* characteristics.

From the current-voltage characteristics it is also possible to extract parameters in the one diode model, described in Section 5.2. These parameters are used to further study the device operation, with components like series resistance, photo generated current, shunt conductance and the junction characteristics itself.

4.2 QE

Quantum efficiency measurements give more in-depth information on the spectral response of the devices, detailing how many electrons are output from the device per photon input. A distinction between external and internal QE can be made. The external QE spectrum relates the number of extracted electrons to the total number of impingent photons, while for the internal QE spectrum the reflection is subtracted before making the QE quota.

The QE spectrum is acquired by irradiating the cell with monochromatic light and measuring the short circuit current. The monochromatic light is typically obtained from a full-spectrum light source using a monochromator with a prism or a grating and filters. This is in order to be able to scan the wavelength of the light from the near UV (~350 nm) to the near IR region (~1200 nm). This is the primary region of interest for photovoltaics, dictated by the range of the solar irradiation and the band gap of the absorber materials used. Most often the signal is chopped into a square waveform, so that it can be separated from ambient light by using a lock-in amplifier. This also enables bias light irradiation, which is important since the cell preferably should be irradiated by approximately 1 000 W/m^2 (i.e. at the level of full solar irradiation). The

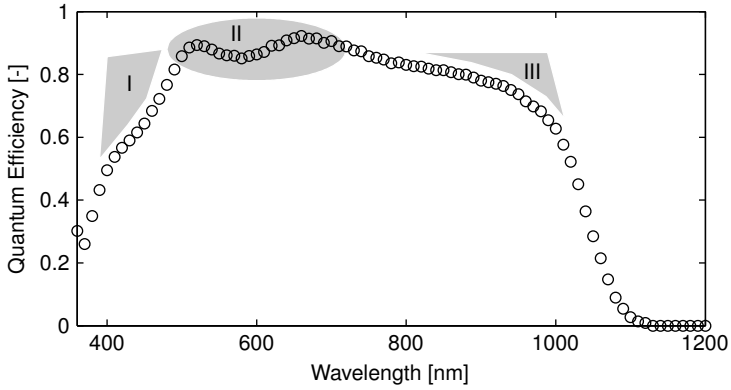

Figure 4.2: Example of a QE measurement plot for a CIGS solar cell. Three areas of interest are marked with roman numerals.

standard measurement procedures are detailed in the IEC 60904-8 standard [2].

With the spectral response of the cell, it is possible to estimate where carriers are generated and how they are collected. For instance, absorption in the CdS buffer layer that does not lead to collected carriers cause a depression of the QE curve in the UV region (see region I in Figure 4.2). Interference in the window layers leads to QE maxima and minima depending on the thickness of these layers (region II). As this reflects the transmittance of the window layers, these features are not present in the internal QE. In the IR region (III), poor QE collection is often present due to the fact that photons at these wavelengths are to a large extent absorbed deep down in the absorber layer, far from the depletion region. The electron-hole pairs generated here run an increased risk of recombining at the back contact as well.

The short circuit current of the cell can be calculated, through:

$$J_{SC} = \int_{\lambda=0}^{\infty} G_{\lambda}(\lambda) QE(\lambda) d\lambda, \tag{4.1}$$

where G_{λ} is the spectral irradiance according to a reference distribution, like the most commonly used AM1.5. This short circuit current value should coincide with the one obtained from a *J-V* curve if the spectrum for the lamp in the *J-V* set up is used, and if the cell is irradiated using a similar light source as bias illumination in the QE measurement.

4.3 *C-V*

C-V measurements, i.e. capacitance–voltage characteristics are, together with *J-V*, the most common measurement method for electronic devices. However, for solar cells the *J-V* dominates as it is intimately connected to the concept of conversion efficiency. *C-V* characterization can be used to estimate depletion region width and carrier density in the devices, using a classic Mott–Schottky plot of $1/C^2$ vs. V. These quantities are important to cell operation and as input to modelling. However, in the case of CIGS cells, the *C-V* method is not as straight forward as with crystalline Si. One problem is that the carrier concentration is not controlled extrinsically by the introduction of doping elements, but intrinsically by defects or defect complexes. This means that the doping may be a function of the applied voltage. The deposition methods used to synthesize CIGS leave little room for controlled adjustment of this property.

There are several methods related to *C-V* measurements, like Deep Level Transient Spectroscopy, Admittance Spectroscopy and Drive Level Capacitance Profiling. They are all more or less based on measurements of admittance at varying frequency and may provide more in-depth information on doping profiles and defect distributions (see e.g. [35, 18, 41]).

4.4 $J(V)_T$

A characterization method that can be used to extract more information on the recombination in the solar cells is temperature dependent *J-V* characterization, or $J(V)_T$. The most important information gained from this method is what recombination path that is the dominant one, in the bulk of the absorber material or at the interface between the absorber and the buffer layer. The different possibilities are illustrated in Figure 4.3. There are two possibilities of bulk recombination, in the quasi-neutral bulk (A) and in the space charge region (B). Furthermore, there is interface recombination (C) and recombination at the back contact (not shown here). In addition to the recombination paths, the tunnelling contribution can be estimated using the $J(V)_T$ method.

J-V measurements are executed at varying temperatures, typically in a span between 200 K and 400 K, often in the illuminated and dark states. The resulting set of curves can be analysed in several different ways, but all the analysis methods are based on the equation for an idealized solar cell:

$$J = J_{00} \exp\left(\frac{-E_a}{AkT}\right)\left(\exp\left(\frac{qV}{AkT}\right) - 1\right) - J_L \tag{4.2}$$

Here J_{00} the saturation current prefactor, is relatively constant with respect to temperature, as is the light induced current J_L. E_a is the activation energy for the dominant recombination process. At the open circuit point, the current through the cell is $J = 0$ while $V = V_{OC}$, so that $\exp(qV/AkT) \gg 1$ and Equation 4.2 can be reformulated to:

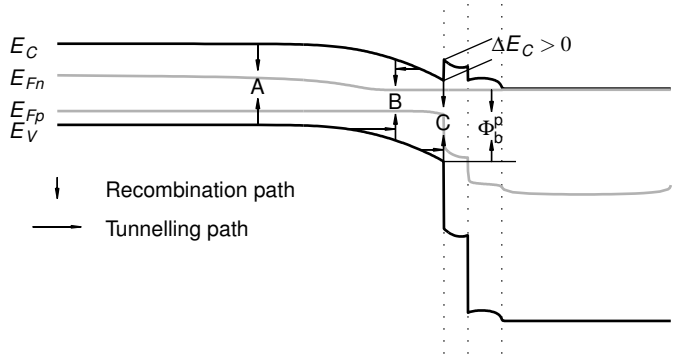

(a) $CuIn_{1-x}Ga_xSe_2$ with $x \approx 0.3$

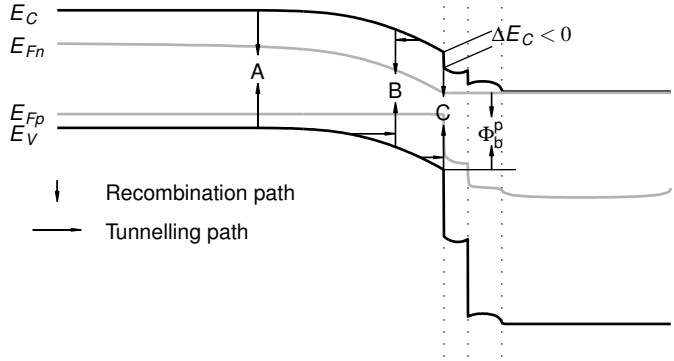

(b) $CuGaSe_2$

Figure 4.3: Band diagram showing the recombination paths in CIGS devices with [Ga]/([Ga]+[In])=0.3 (a) and for pure CGS (b). The diagrams are simulated with the baseline case from Table 5.1, an applied voltage of 0.3 V and AM1.5 illumination.

$$V_{OC} = \frac{E_a}{q} + \frac{AkT}{q} \ln\left(\frac{J_L}{J_{00}}\right) \tag{4.3}$$

The temperature dependence of the activation energy, E_a, can be taken into account assuming that it is linear with temperature according to $E_a = E_a^0 - CkT$. This assumption is reasonable since the temperature dependence of the band gap energy is close to linear [68] in the temperature region where $J(V)_T$ typically is performed. Consequently the V_{OC} can be expressed as:

$$V_{OC} = \frac{E_a^0}{q} - \frac{kT}{q}\left(C - A\ln\left(\frac{J_L}{J_{00}}\right)\right) \tag{4.4}$$

Assuming that $C - A\ln(J_L/J_{00})$ is constant with respect to temperature, the V_{OC} can be plotted versus kT/q, and thus the activation energy, E_a^0 (extrapolated to $T = 0\,\mathrm{K}$), can be extracted. This method of extracting the activation energy is useful only when the ideality factor is independent of temperature, which is rarely the case with CIGS-based cells.

A more advanced method of extracting the activation energy involves determining the one diode model parameters (see Section 5.2). From the expression for the saturation current, $J_0 = J_{00}\exp(-E_a/AkT)$, the following expression can be derived:

$$\ln\left(\frac{J_0}{J_{00}}\right) = \frac{-E_a}{AkT} \tag{4.5}$$

Again, if the activation energy is assumed to vary linearly with temperature, this can be reformulated to:

$$A\ln\left(\frac{J_0}{J_{00}}\right) = -\frac{E_a^0}{kT} + C \tag{4.6}$$

$A\ln(J_0/J_{00})$ can be plotted versus q/kT so that the activation energy can be extracted as the slope of the linear plot. One difficulty here is to obtain the quantity J_{00}. It can be accomplished by making a non linear fit to measurement data according to

$$A\ln(J_0) = A\ln(J_{00}) - \frac{E_a^0}{kT} + C, \tag{4.7}$$

where the quantities E_a^0, $\ln(J_{00})$ and C are used as variables. Here, the activation energy is obtained directly, but the previous mentioned plot (cf Equation 4.6) can be used to make certain that the plot is linear, as it should be.

Depending on what recombination path is the dominant one in the cell, the activation energy should be equal to either the band gap or the minority hole barrier at the interface between the absorber and the buffer layer, Φ_b^p. In the case of $E_a = E_g$, the recombination path most likely to dominate current transport is in the bulk of the absorber (see paths A and B in Figure 4.3). On the other hand, if $E_a = \Phi_b^p$ the cell characteristics is considered to be interface recombination controlled (path C) [66]. Furthermore, the contribution from tunnelling can be estimated from the temperature dependence of the ideality factor, see for instance [63].

Although the $J(V)_T$ method can provide more insight into the recombination mechanisms that govern current transport in thin-film solar cells, there are some difficulties involved in applying the various analysis methods. One difficulty lies in the fact that when analysing J-V characteristics measured at low temperatures, there are more non-idealities that come into play. One of these effects, roll-over or blocking behaviour at low temperatures, is clearly illustrated in Figure 4.4, where two sets of curves are displayed; one showing

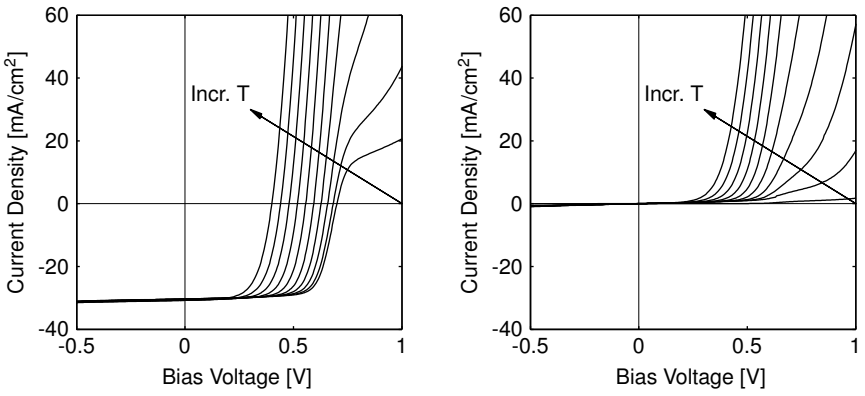

(a) Illuminated *(b)* Dark

Figure 4.4: J-V curves at temperatures between 200 K and 380 K in increments of 20 K.

the illuminated state (a) and the other one the dark state (b), for temperatures between 200 K and 380 K. The curves at low temperatures are severely distorted, and this makes it difficult perform the model fits needed for the $J(V)_T$ analysis. In these cases, the one diode model does not apply and a more complex model would have to be used. However, with most cells there is a suitable temperature span where the one diode model does apply and the analysis can be carried out.

An additional difficulty in the analysis of $J(V)_T$ data is that in certain circumstances the activation energy, E_a, may become larger than the band gap, even if interface recombination dominates the current transport. This caveat was raised by Jonas Malmström in his thesis [51], where he showed that a result of $E_a \geq E_g$ does not automatically signify bulk recombination dominance. It is especially true if the ideality factor varies strongly with temperature. However, an activation energy $E_a < E_g$ does mean that interface recombination is the dominant path.

As en example of applications of the $J(V)_T$ method, it is used in Paper VII to analyse cells with alternative buffer materials. The study on CIS- and CIGS-based devices with ZnO as buffer layer directly on the absorber showed that for CIS cells, the dominant recombination was in the bulk of the absorber. This is the normal mode for CIGS cells with low to medium Ga content and CIS, for standard CdS buffer layer. For CIGS cells with medium Ga content and direct ZnO, the dominant recombination path was at the interface, which is the common mode of CGS/CdS devices as shown in, e.g., [67]. This is most likely due to the fact that there is a negative conduction band offset, ΔE_C, between the absorber and the buffer layers, as illustrated in Figure 4.3b for the case of CGS/CdS [91]. The situation at the absorber buffer interface is similar in the case of CIGS/ZnO, with enhanced interface recombination as result.

5. Modelling and Simulations

There are several different ways of modelling solar cells, and each type of modelling can naturally by performed with varying degree of detail. In this chapter a couple of approaches to modelling and simulation of thin-film CIGS solar cells are described.

5.1 Modelling Methods

The different ways of modelling solar cell devices can be divided into two major groups, analytical models and numerical models. In the analytical ones, an equivalent circuit is modelled, where the different parts correspond to physical entities of the device. This way of modelling electronic components is common in semiconductor device physics, e.g., the Ebers-Moll model of a bipolar transistor [78, chapter 3]. In order for the model to be relevant, its components must have physical relevance. Although it may be tempting to increase the number of parameters in the model, with the result that the quality of the fit improves, this involves a trade-off between how exact measurement data can be reproduced by the model and how many model parameters are used. A model with more parameters than can be justified in physics may provide excellent fits, but with little relevance in the result. The model used here is the one diode model shown in Figure 5.1.

The second type of modelling described here, using numerical models, most often entails solving of partial differential equations using either finite difference or finite element methods. For thin-film solar cells there are several 1-D simulation packages that utilize the finite difference method, with slight differences in approach. Finite differences can also be used in 2-D and 3-D, but finite element analysis is more flexible with complex geometries and is the method primarily used in this work.

Furthermore there are hybrid methods that take advantage of both the primary modelling methods. One such method is when an analytical model is used as a boundary condition to a numerical simulation of e.g. the current distribution in the front contact (see Section 5.4). This type of simulation can also be performed with a network approach, where the one diode model is extended to a multi-diode network, and subsequently the output characteristics is computed using numerical methods.

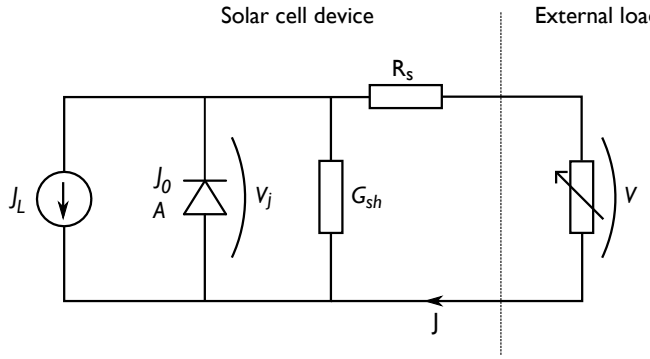

Figure 5.1: The one diode model describes a solar cell device, using a *p-n* junction (A, J_0), a current generator (J_L), a shunt conductance (G_{sh}) and a series resistance (R_s).

5.2 The One Diode Model

The most common analytical model for a solar cell, at least in the CIGS cell case, is the one diode model described in Figure 5.1. There are alternatives, like the two diode model that is often used to model crystalline silicon solar cells. Other alternatives, incorporating more circuit elements can also be constructed, for instance with a blocking back contact barrier.

The one diode model, used here, consists of a *p-n* junction, described by the saturation current (J_0) and the ideality factor (A), a current generator (J_L), a shunt conductance (G_{sh}) and a series resistance (R_s). This model is illustrated in Figure 5.1 and its J-V characteristics can be described analytically by the equation

$$J = J_0 \left(\exp\left(\frac{q\,(V - JR_s)}{AkT} \right) - 1 \right) + G_{sh}\,(V - JR_s) - J_L \qquad (5.1)$$

The three terms on the right hand side in Equation 5.1 represent three parallel currents, which correspond to the diode current, the shunt current and the photo-generated current in the equivalent circuit. The voltage over these three components is given by $V_j = V - JR_s$, the junction voltage.

The five parameters of Equation 5.1 can be extracted from fitting the model to experimental data. This is the essence of the analytical modelling. The extracted parameters are used to evaluate different respects of device performance. As an example of a direct connection between one diode model parameters and physical effects, an abnormally large shunt conductance can easily be identified from the G_{sh} parameter.

There are several ways of extracting the one diode model parameters from measurement data, i.e. from J-V characteristics. It can be done with several consecutive linear fits to different representations of different parts of the J-V curve. Firstly, the shunt conductance can be extracted from the inclination of the linear part of the J-V curve at $V < 0$. The series resistance can then be

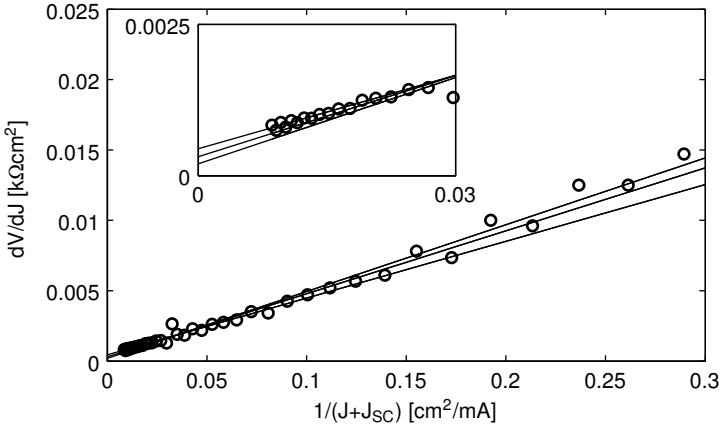

Figure 5.2: In this extraction of the series resistance of the one diode model, the three different fits were made in three different intervals, [0 0.1], [0 0.2] and [0 0.3].

extracted from the forward part of the curve and subsequently the effects of shunt conductance and series resistance can be removed from the *J*-*V* curve data, so that the ideality factor and the saturation current can be extracted from a lin-log plot of J vs. V.

These sequential fits are often accurate enough, but have the inherent problem that a number of fitting regions have to be decided by the user. This introduces a potential for errors, depending on the sensitivity of the least squares fit to the extent of the chosen region. In Figure 5.2, the series resistance value is extracted from the plot of dV/dJ versus $1/(J+J_{SC})$, where the most important part is at the lower left, i.e. the forward part of the *J*-*V* curve. The R_s value is read at the intersection of the extrapolation and the y-axis, and this value may vary by a factor of two depending of how large the fitting region is. There is another potential source of error here. The quantity dV/dJ that is plotted in Figure 5.2 has to be computed numerically. There is an additional way of determining the ODM parameters, based on a series of measurements at different illumination. The method takes advantage of the fact that the series resistance does not influence the V_{OC} value. This enables a lumped R_s value to be determined accurately, but only if the condition of superposition is fulfilled. This, and other methods for establishing the series resistance parameter are reviewed in [61].

An alternative way of extracting these model parameters is to fit the whole model to the measurement data in one least squares fit procedure. A problem that arises here is the strongly varying slope of the *J*-*V* curve, which creates difficulties with the standard least squares fit where it is assumed that the error in J is normal distributed. This has the effect that the forward part of the curve, where the slope is high, will be strongly overemphasized in the fit.

Instead, a weighted least squares fit must be used so that errors in the voltage measurement also are taken into account. This can be accomplished with the orthogonal distance regression (ODR) method [14], where the fit is weighted by the inverse of the measurement uncertainty at the respective measurement points. This uncertainty is combined from the measurement uncertainties in current density and voltage according to:

$$\sigma\left(J\left(V\right)\right) = \sigma\left(J\right) + \frac{dJ}{dV}\sigma\left(V\right) \tag{5.2}$$

In this way the strongly varying slope is taken into account, and the fit is not over-emphasized in the high slope region. With the ODR fitting method, it is thus possible to separate the five one diode model parameters from a single fit. Because of the exponential function in the one diode model, the J_0 varies rapidly and may change by several orders of magnitude during a fitting procedure. This can be remedied by letting the fitting algorithm use $\ln\left(J_0\right)$ as a model parameter instead of J_0. Thus, the convergence is drastically improved.

One concern with this kind of model-fitting to measurement data is that the co-variance of parameters may be high, and thus lead to erroneous fits. In the case of fitting the one diode model to *J-V* data, this occurs mainly between the $\ln\left(J_0\right)$, A and R_s parameters, but with the ODR method the effect of an external discrete resistor can readily be separated from the cell characteristics, showing that the co-variance between A and R_s is not a significant problem. As with the sequential fits, the fitting region must be decided by the user, but ideally the result should be the same for all parts of the curve. This is, however, not the case for some *J-V* curves where there are additional non-idealities like the ones mentioned in conjunction with $J(V)_T$ in Section 4.4.

The one diode model parameters can be used to characterize the device and to understand what losses are present. Another important use for the one diode model parameters is to provide a basis for recombination analysis in temperature dependent *J-V* measurements, $J(V)_T$. Although the activation energy for the dominant recombination process can be determined from the temperature dependence of the open circuit voltage, it is more accurate to use the saturation current density. This is especially true when the ideality factor varies with temperature, as is most often the case with CIGS cells. Furthermore, the ODM parameters have to be used when analysing the dark $J(V)_T$ characteristics, since there is obviously no possibility to analyse the V_{OC}.

5.2.1 ODM Modelling for Degradation Studies

Degradation studies on solar cells most often entails closely monitoring cell characteristics, while exposing them to accelerated test conditions. Looking at the solar cell parameters, V_{OC}, J_{SC}, FF and η, some trends can be traced, but from these it is difficult to obtain any information about what is changed in the cell. For instance, a FF loss can be due to a number of underlying effects such as shunt, resistance or recombination effects.

These effects can be separated using the ODM parameters instead. When a CIGS solar cell is degraded by damp heat treatment, there are most often losses in open circuit voltage and fill factor, while the short circuit current essentially remains intact [89, 34, 52, 71]. Using the ODM modelling it is possible to separate the effect of increased recombination in the cell from that of increased series resistance or shunt conductance. This subject is elaborated on further in Section 6.2.1

5.3 Numerical Device Modelling

In numerical device simulations in general, partial differential equations are solved subject to certain boundary conditions. Compared to the analytical modelling that uses macroscopic circuit elements, the numerical device simulations are used to calculate fundamental physical properties, like electrical potential and electron and hole concentrations. This may provide more information on how material parameters influence device characteristics.

In the numerical model described here, as in all semiconductor device simulations, the Poisson equation

$$\nabla(\varepsilon_r \varepsilon_0 \nabla \Psi) = q(p - n + N_D - N_A) \tag{5.3}$$

is solved with appropriate boundary conditions, together with the steady-state continuity equations for electrons and holes:

$$\nabla \mathbf{J}_n = -q(G - R_n) \tag{5.4}$$

$$\nabla \mathbf{J}_p = +q(G - R_p) \tag{5.5}$$

Ψ is the electric potential while p and n are the carrier densities. N_A and N_D denote ionized doping densities, acceptors and donors. J_n and J_p are the electron and hole current densities, respectively, while G is the generation rate and R is the recombination rate.

These three equations (5.3 – 5.5) are the most fundamental semiconductor differential equations. Poisson's equation is one of the Maxwell equations, while the continuity equations state that the net inflow of charge carriers into a volume must equal the net generation, i.e. the difference between generation and recombination, so that no charge carriers materialize out of thin air.

Furthermore, there are the current density equations that create a link between carrier densities, current densities and potential through:

$$\mathbf{J}_n = q\mu_e n \nabla \Psi + qD_e \nabla n \tag{5.6}$$

$$\mathbf{J}_p = q\mu_p p \nabla \Psi - qD_p \nabla p \tag{5.7}$$

Here the two currents, drift and diffusion, are added up to the total current densities for electrons (Equation 5.6) and holes (Equation 5.7).

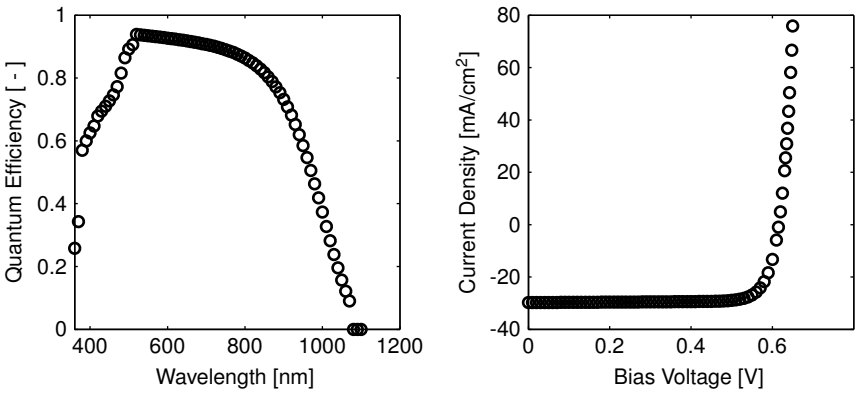

(a) *(b)*

Figure 5.3: An example of simulated QE and *J-V* characteristics using the parameters given in Table 5.1 in AFORS-HET.

5.3.1 1-D Device Simulation Software

There are several device simulation packages that readily simulate multi-layer heterojunction solar cells in one dimension, including AMPS [22], SCAPS [13], AFORS-HET [23], ASPIN [80] and ASA [87]. These have been used in several important studies over the past 20 years and have furthered the understanding of the operation of thin-film solar cells. All of the mentioned simulation software packages utilize the finite difference method, which approximates the partial differential equations to be solved on a line from back to front through the cell structure. This line, and thus the partial differential equations, are discretized into N segments, resulting in $3N$ non linear equations that are solved numerically.

One difficulty with numerical device simulation of CIGS solar cells is the lack of measurement values for some of the physical quantities that the simulations are based upon. While several of them, like band gap, dielectric constant, optical properties, electron affinities and more, are available from literature for most materials used in CIGS devices, others are difficult to measure. This is especially true for defect characteristics and interface properties (see e.g. [19]). For this reason, studies using numerical simulations most often use a baseline case, with the most likely set of parameters for a baseline cell, and then parameters are varied one at a time in order to study specific effects. There have also been attempts at inverse modelling, obtaining physical parameters by fitting models to experimental data [93].

Examples of modelling studies that have furthered the knowledge about the inner workings of CIGS devices include the effects of increased conduction band minimum at the absorber/buffer interface when the band gap is increased [26]. This type of band gap grading was also studied in [74]. The blocking

Table 5.1: *An example of parameters used in a baseline 1-D simulation. The parameter set has been compiled from a number of sources, most notably [25].*

Quantity		Layers			
		CIGS	CdS	ZnO	ZAO
ε_r	[-]	13.6	10	9	9
χ	[eV]	4.1	3.8	4	4
E_g	[eV]	1.15	2.4	3.3	3.3
μ_e	[cm^2/Vs]	100	100	100	100
μ_h	[cm^2/Vs]	25	25	25	25
N_c	[cm^{-3}]	2.22×10^{18}	2.22×10^{18}	2.22×10^{18}	2.22×10^{18}
N_v	[cm^{-3}]	1.78×10^{19}	1.78×10^{19}	1.78×10^{19}	1.78×10^{19}
N_A	[cm^{-3}]	3.5×10^{16}	0	0	0
N_D	[cm^{-3}]	0	3.5×10^{17}	1×10^5	1×10^{18}
v_e	[cm/s]	1×10^7	1×10^7	1×10^7	1×10^7
v_h	[cm/s]	1×10^7	1×10^7	1×10^7	1×10^7

behaviour of CIGS cells at decreased temperature has also been studied [81], as well as the cross-over between illuminated and dark *J-V* characteristics [57].

An example of a 1-D simulation of a CIGS cell is shown in Figure 5.3, where the parameters given in Table 5.1 are used to compute QE and *J-V* characteristics with AFORS-HET. As mentioned previously, not all parameters are well known, but are estimated. The parameter set in Table 5.1 has been compiled from various sources, e.g. [70], [57] and [25] where a baseline case is presented.

5.3.2 2-D Device Simulations

Although 1-D simulations of thin-film solar cells can be very useful in determining the effects that different parameters have on device performance, it is of little use when studying other effects like discrete shunts, weak diode areas, material inhomogeneities, contact geometries and grain boundaries. In these cases the cells need to be simulated in two or three dimensions. There are not any fundamental differences between simulating solar cell devices in one or more dimensions, but it does complicate the discretization and solving of the semiconductor equations. The difference in the equations is simply that the functions involved are all functions of two or three spatial quantities (e.g. x, y in 2-D):

$$\nabla\left(\varepsilon_r(x,y)\varepsilon_0\nabla\Psi(x,y)\right) = q\left(p(x,y) - n(x,y) + N_D(x,y) - N_A(x,y)\right) \quad (5.8)$$

$$\nabla\mathbf{J}_n(x,y) = -q\left(G(x,y) - R(x,y)\right) \quad (5.9)$$

$$\nabla \mathbf{J}_p(x,y) = +q\,(G(x,y) - R(x,y)) \tag{5.10}$$

The Equations 5.8 through 5.10 are solved with the boundary conditions given in Equations 5.11 through 5.13 at the back contact and 5.14 through 5.16 at the front contact. n_0 and p_0 are the equilibrium carrier densities.

$$\Psi|_{\text{back}} = V_a \tag{5.11}$$
$$J_n|_{\text{back}} = +qS_n^b\,(n|_{\text{back}} - n_0|_{\text{back}}) \tag{5.12}$$
$$J_p\big|_{\text{back}} = -qS_p^b\,(p|_{\text{back}} - p_0|_{\text{back}}) \tag{5.13}$$

$$\Psi|_{\text{front}} = 0 \tag{5.14}$$
$$J_n|_{\text{front}} = +qS_n^f\,(n|_{\text{front}} - n_0|_{\text{front}}) \tag{5.15}$$
$$J_p\big|_{\text{front}} = -qS_p^f\,(p|_{\text{front}} - p_0|_{\text{front}}) \tag{5.16}$$

Here, the quantities S_n and S_p are the recombination velocities at the contact surfaces. The f and b superscripts denote the front and back boundaries, respectively. The quantities solved for are Ψ, n and p. From these and the material parameters, band diagrams and currents can be calculated.

In this work, 2-D device simulations are performed using the finite element method, instead of the finite difference method used in the 1-D simulation packages. The modelling, discretization and calculations are performed using the software package Comsol Multiphysics (see Paper I).

The variations in carrier density between the different semiconductor layers in a heterojunction thin-film solar cell can be very large, many orders of magnitude. This is the case in CIGS cells when comparing the hole density in the p-type CIGS layer and in the heavily n-type ZAO window layer. Partly, these extreme variations are in the nature of semiconductor physics, but emphasized in the CIGS solar cell structure due to the large band gap of the ZAO. With a large band gap the minority carrier density becomes extremely small, since there is an exponential relationship between intrinsic carrier density and the band gap, $n_i = \sqrt{N_C N_V}\exp(-E_g/2kT)$. As an example, the intrinsic carrier density of ZnO, with a band gap of 3.3 eV, is in the order of 10^{-9} cm^{-3}. This, with the high doping of the ZAO, leads to an extremely low minority carrier density as exemplified in Figure 5.4a, where the carrier densities for a typical CIGS structure is plotted. The large variation is difficult to handle in the finite element method, since it results in an ill-conditioned coefficient matrix for the equation system that is to be solved. In order to go around this problem the quasi Fermi levels, illustrated in Figure 5.4b, are used instead of the carrier densities according to:

$$n = n_i \exp\left[\frac{E_i - E_{Fn}}{kT}\right]$$

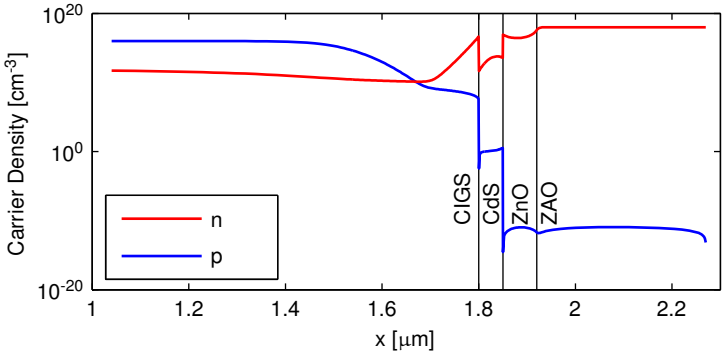

(a)

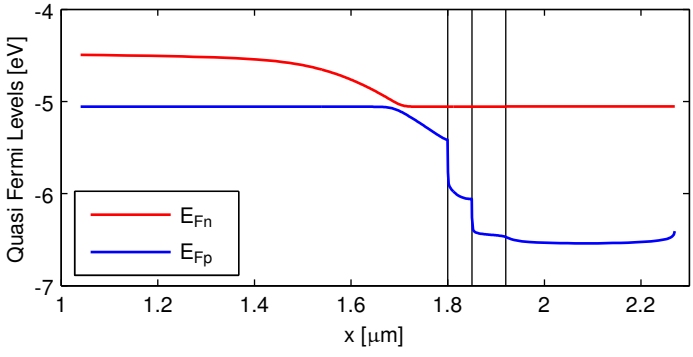

(b)

Figure 5.4: An example of simulated carrier densities (a) and quasi Fermi levels (b) for a typical CIGS cell under illumination (from baseline case in Table 5.1).

$$p = n_i \exp\left[\frac{E_{Fp} - E_i}{kT}\right]$$

This means that Poisson's equation (5.8) becomes:

$$\nabla(\varepsilon_r \varepsilon_0 \nabla \Psi) = q\left(n_i \exp\left[\frac{E_{Fp} - E_i}{kT}\right] - n_i \exp\left[\frac{E_i - E_{Fn}}{kT}\right] + N_D(x,y) - N_A(x,y)\right) \quad (5.17)$$

In this way, the electric potential together with the quasi Fermi levels, E_{Fn} and E_{Fp}, are the quantities solved for, while the other quantities are calculated from the input parameters.

5.3.3 Results from 2-D device modelling

The CIGS absorber material is far from a well-behaved single crystalline elemental semiconductor, but instead a poly crystalline quaternary compound where the composition may vary with position. Depending on deposition process, the material will contain inhomogeneities. The most common of which is the band gap grading, e.g. present in the three-stage co-evaporation process where a double grading normally is acquired [24]. Furthermore, lateral fluctuations in the band gap energy has been observed by microscopic photoluminescence studies [30]. These fluctuations may be due to variations in composition between grains, or between grains and grain boundaries.

In Paper I, 2-D simulations of solar cell cross-sections with variations in material parameters, like the ones mentioned in the previous section, are performed. Fluctuations in the band gap are introduced as a superposition onto a base line case similar to that described by Table 5.1. These fluctuations, in the form of randomized deviations from the original band gap, are entered as two-dimensional functions of depth and one lateral coordinate in the cell structure. They are characterized by the standard deviation, σ_g. An example of such a function is shown in Figure 5.5. A series of simulations with varying magnitude of fluctuations is calculated. From [27], the influence on the open circuit voltage by fluctuations in the band gap can be calculated analytically:

$$V_{OC} = V_{OC}^0 - \frac{\sigma_g^2}{2qkT}, \tag{5.18}$$

where V_{OC}^0 is the open circuit voltage with constant band gap energy. This analytical model is confirmed by the simulations, showing that the voltage decrease is moderate for fluctuations of $\sigma_g < 20$ meV, while it increases rapidly for larger fluctuations.

In addition to the band gap fluctuations, a series of simulations with different fluctuations in mid-gap trap density in the CIGS was also calculated. The result of this is similar compared to the results from fluctuating band gap, with little change in the *J-V* curve for variations in trap density of less than 5×10^{16} cm^{-3}, but with rapidly increasing deterioration of the cell performance for higher values. This is illustrated in Figure 2 of Paper I.

One of the most important strengths with the implementation of 2-D simulations that is described in Paper I is that all material properties can be entered into the simulations freely, as two dimensional functions of x and y. It is also quite straightforward to implement geometric features like a rough interface between the absorber and the buffer layer.

A downside of the implementation is that a large number of mesh points, and thus a large number of degrees of freedom (DOF), has to be used in order to resolve the features of the cell structure and the rapidly varying parameters. This makes the calculations computationally heavy, and with a reasonably modern desktop computer (AMD Athlon 64 X2 4400+ with 4 GB of RAM) the simulation of one *J-V* curve, for a 1 μm wide cross-section, takes approx-

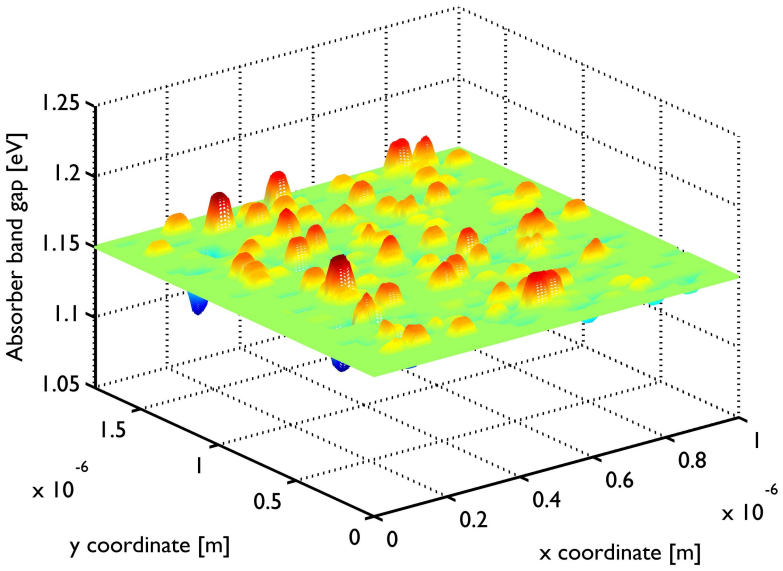

Figure 5.5: Band gap fluctuations of $\sigma_g = 10\,\text{mV}$ as used in the 2-D simulations of cells with varying material parameters.

imately 25 minutes. Increasing the extent of the simulations, to larger cross-sections or with complex geometric variations, would increase the number of DOF and the computation time.

5.4 Hybrid Simulation Models

The numerical simulations described in the previous section are reasonably straightforward in one dimension, manageable in two dimensions, but difficult to perform in three dimensions. This means that they cannot be used for applications like simulations of complete cell structures with a current collecting grid, or for point defects. In order to accomplish this kind of modelling, a hybrid model can be used.

One way of combining numerical and analytical modelling into a hybrid model is to use the one diode model, described in Section 5.2, as a boundary condition in a numerical simulation of steady state electrical conduction in the front contact layers. This can be described as the generalization of a network model to an infinite number of one diode models.

5.4.1 Network Model

The real solar cell device can be viewed as a very large number of small solar cells that are connected in parallel through the back and front contact layers.

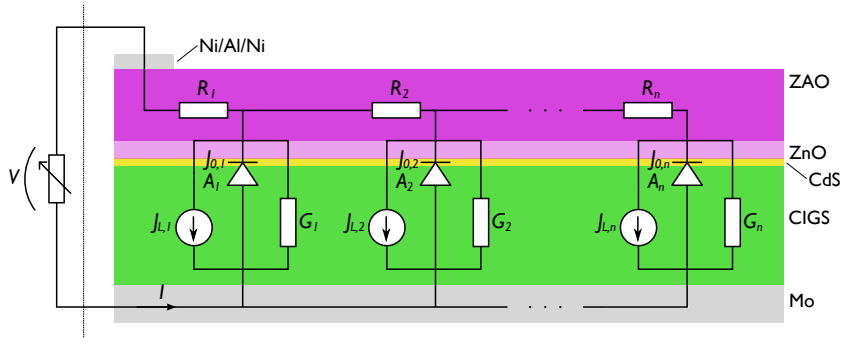

Figure 5.6: Schematic drawing of a two dimensional network model with n one diode model subcells in parallel.

This situation can be approximated using a network of discrete devices and wires that connect them, a so called network model, which is illustrated in Figure 5.6. This type of modelling has not been performed within this work but should be mentioned for completeness. Several authors have used this kind of network model to study effects of inhomogeneities and module cell optimization in CIGS-based solar cells [11, 40, 27, 10]. Each discrete diode is represented by a set of parameters from the one diode model, and the current and voltage distributions can be calculated numerically using a software package like SPICE.

One difficulty with the network model is that the cell, which is a continuous entity, is modelled as a network of discrete components. This means that physical quantities like resistivity and layer thickness, as well as geometric constraints, must be translated into the network model. The process of discretizing the semiconductor layer in this way may not be a straightforward task. A more intuitive way of modelling this, from device geometries and material quantities, is presented here in Section 5.4.4.

5.4.2 Model Generalization

If the number of subcells in the network model is increased towards infinity, the one-diode models will converge to a continuous, distributed diode. The network of resistors connecting the subcells will converge to a continuous layer of conductive material. One way of approaching this limit is to simulate the potential in the contact layers using, e.g., the finite element method. In this way, the one diode model action of the subcells in the network is modelled as a continuous boundary condition over the bottom surface of the window layer. While the modelling is continuous, the solution is discretized in the form of a mesh.

The potential distribution of the front contact is acquired by solving

$$\nabla\left(\varepsilon_r\varepsilon_0\nabla\Psi\right) = 0 \tag{5.19}$$

for steady state electrical conduction. Ψ is the electric potential and ε_r is the relative dielectric constant of the contact layer material. Both these quantities are functions of the spatial variables. The boundary conditions used on the bottom surface are described by:

$$J_{in}(x,y,0) = J_0 \left[\exp\left(\frac{q\,(V_a - \Psi(x,y,0) - R_s J_{tot})}{AkT} \right) - 1 \right] + G_{sh}\,(V_a - \Psi(x,y,0) - R_s J_{tot}) - J_L \quad (5.20)$$

Here the quantity $J_{in}(x,y,0)$ is the current input at the position (x,y) on the bottom surface of the modelled contact layers, defined here as $z = 0$. The one diode model parameters that provide the operating characteristics for the underlying distributed diode can be given as constants or as functions of x and y. Although Equation 5.20 essentially is the one diode model, there is a slight difference between it and Equation 5.1. In the boundary condition given here, the series resistance is not defined on a local level as the other parameters but as global series resistance that influences the whole cell. To this, the series resistance effect of the front contact is added in the simulation. The total current, J_{tot}, which is multiplied by the series resistance parameter, is given by:

$$J_{tot} = \int_{\text{contact}} \mathbf{J} \cdot d\mathbf{S} \quad (5.21)$$

i.e. the total current through the cell. This means that the voltage $V_j = V_a - \Psi(x,y,0) - R_s J_{tot}$ is the junction voltage experienced in the position (x,y) with an applied bias voltage of V_a.

This way of introducing the solar cell action provides excellent flexibility in the modelling, with few constraints on spatial variations in material parameters. Geometries, with cell shape and contact structure patterns, can also be modelled quite freely.

5.4.3 2-D Hybrid Modelling

The simplest implementation of the hybrid simulation is when a 2-D cross section of a module type cell is modelled. Without material inhomogeneities this is essentially a 2-D situation with the current flowing perpendicularly to the cell's long side (as it is supposed to in the module design). This kind of cross section model is shown in Figure 5.7a, where the ZnO and ZAO layers are seen, with current inflow from the right edge of the upper (ZAO) layer and out through the bottom. In a module, the contact at the side edge of the ZAO layer would feed into the interconnect structure described in Section 3.2.

Because of the very high aspect ratio of the simulated structure, on the order of 10 000:1, it is difficult to use a model to scale. If the cell cross section were to be modelled by a rectangle with a height of 100 nm and a width of a few millimetres, the minimum element size in the discretization of the geometry

would be governed by the film thickness (100 nm). This would result in a very large number of elements along the width of the cell, causing a significant slow-down of calculations. The issue can be remedied by using an anisotropic scaling of the geometry, making it thick enough for the number of DOF to be manageable. At the same time the properties of the material must be scaled anisotropically, with an increase in the conductance in the y-direction (vertically in the cell structure) paired with a decrease of the conductivity in the x-direction (laterally) by the same factor.

This 2-D hybrid modelling of cross-sections has not been studied extensively in this work. More on the technique and applications, with a slightly different but essentially equivalent method, can be found in [38].

5.4.4 3-D Hybrid Modelling

As mentioned in the previous section, the cross-section of a module cell is very much suited to 2-D simulations, since little current flows parallel to the cell's long side. The situation for a laboratory scale cell, with a current collecting grid on top of the ZAO layer, is quite different and needs 3-D simulations. This is also true for a module type cell with varying material properties.

Similar to the extension of numerical device simulations from one to two dimensions, there is no fundamental difference between hybrid simulations in two or three dimensions. The most important difference is that the complexity of the calculations, the number of degrees of freedom, increases drastically.

5.4.5 Results from hybrid modelling

The hybrid modelling can, for example, be used to investigate the effects of the distributed series resistance in laboratory cells, and how it influences the extraction of one diode model parameters. One way of monitoring cell performance, and analysing cell behaviour is to study ODM parameters, as discussed in Section 5.2. However, this method has its constraints in the fact that the simple ODM only uses a lumped series resistance, while different parts of the real cell will experience different electrical potential.

In Paper II, the effects of front contact resistance on extracted diode parameters are studied. In the hybrid model, the cell can be thought of as a very large number of small subcells connected in parallel. Since these are located at different positions in the cell they will experience different series resistance as the distance to the nearest grid finger or contact point varies. Consequently, their respective operating characteristics will be different even if the cell layers are perfectly homogeneous. This manifests itself in a variation of the electric potential over the cell, as can be seen in Figure 5.7b When adding up the contributions, this variation in series resistance will lead to a distortion of the complete J-V curve, as the shapes of the different subcell curves are different. If ODM parameters are extracted from these curves, the distortion will lead to a misinterpretation of the model parameters, that primarily has an effect on the A and the J_0.

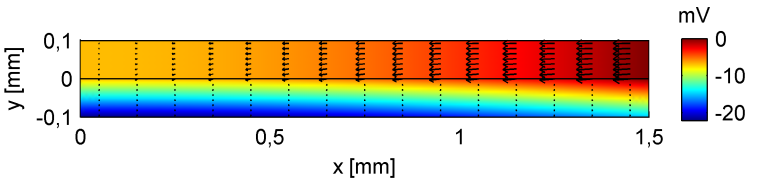

(a) 2-D module cell

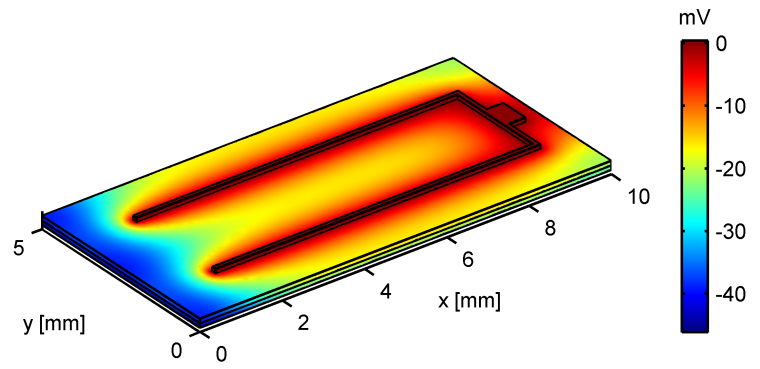

(b) 3-D laboratory cell

Figure 5.7: Two examples that show the resulting potential in a cross-section of module cell (a) and in a laboratory scale cell with current collecting grid (b)

With an increased resistivity or decreased thickness in the ZAO, resulting in higher sheet resistance, the effects on extracted ODM parameters increases. Conversely, a current collecting grid lowers the effect. This means that in cells with highly resistive front contact material, or with a poor current collecting grid, extracted ODM parameters must be treated cautiously. However, with normal laboratory scale cells, the current collecting grid ensures that the effects of lateral current distribution are not very severe. Consequently, the increased ideality factors and saturation currents seen in cell degradation (see Papers V and IV) are not an artefact but actual changes in the junction characteristics.

On the other hand, for module cells, as studied in e.g. [45], the effect of lateral current distribution on the extracted ideality factors and saturation currents play a significant role. The increases in A and J_0 observed there can be explained by the artificial increase from the front contact resistivity. In this kind of study, it is difficult to separate the effects of increased sheet resistance from that of changed junction properties. For more one these effects, see Section 6.2.2.

In Paper III the hybrid model is used to study lateral inhomogeneities in material properties and discrete shunt defects in module type cells. When manufacturing thin-film solar cells and modules, there will always be variations in film properties over the surface, especially for large area devices. In all the layers in the structure these types of fluctuations may occur in, e.g., the thickness

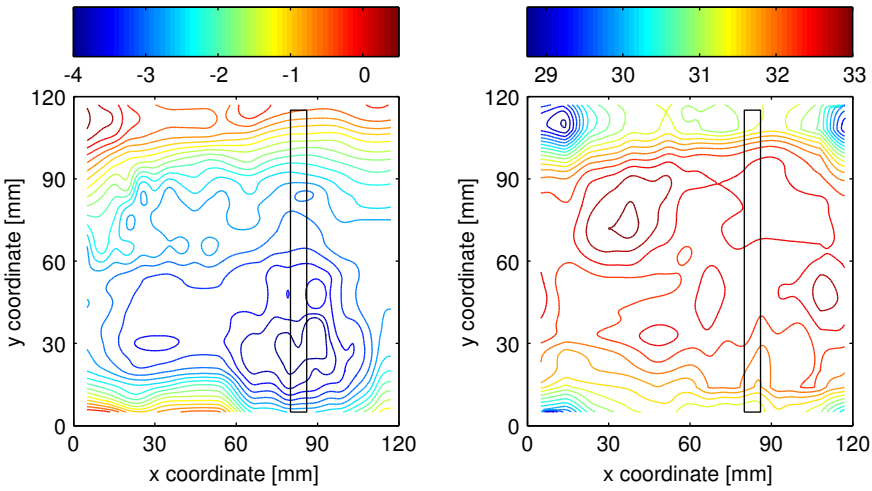

(a) $\log\left(J_0\ [\mathrm{mA/cm^2}]\right)$ *(b)* $J_L\ [\mathrm{mA/cm^2}]$

Figure 5.8: The logarithm of the saturation current, J_0 (a), and the light-induced current, J_L (b), mapped over the surface area of a 12.5 cm $\times$ 12.5 cm.

or in material quantities like band gap or trap density. As mentioned in Section 5.3.3, band gap fluctuations are common due to compositional variation in the CIGS compound. The variations that occur vary greatly with the type of deposition used, e.g. co-evaporation, selenization from metal precursors or from screen-printed nano-composites.

Such variations were mapped for a 12.5 cm $\times$ 12.5 cm substrate, where *J-V* characteristics were recorded for 288 subcells of 0.5 $\mathrm{cm^2}$ surface area [94]. From these *J-V* characteristics, ODM parameters were extracted and interpolated to 2-D functions, exemplified in Figure 5.8.

In Paper III module type cells are simulated for different ZAO layer thicknesses and for different cell widths, using the parameter maps in Figure 5.8 in an inhomogeneous case. The optimization of cell efficiency is studied for this and a homogeneous reference case. For the relation between ZAO layer transmittance and sheet resistance the semi-empirical Beer-Lambert model of [38] is used. The effects of the inhomogeneous material parameters on the optimization of cell width and ZAO sheet resistance are limited, with some benefits of using wider cells in the inhomogeneous case. A wider cell screens part of the areas with worse material quality, offsetting the increased series resistance incurred.

Furthermore, module cells are simulated with discrete shunt defects, modelled as circular wells in the absorber layer where the ZnO/ZAO double layer meets the back contact Mo. The size and position of the shunts and the thickness of the ZnO layer are varied. The position of the defects is not a critical parameter, as it had little influence except for at the very edges of the cell.

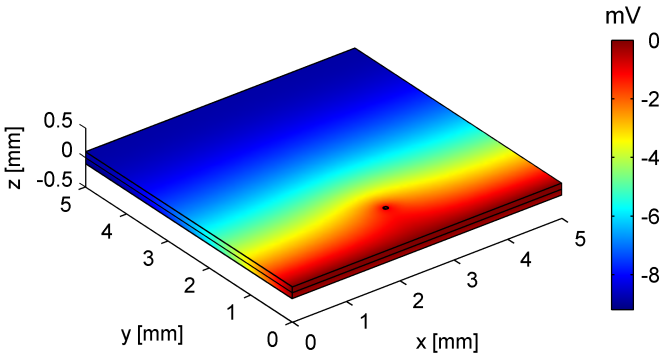

Figure 5.9: An example of a 30 µm shunt modelled in a module type cell, as the ones studied in Paper III. The applied voltage is $V_a = 0.4$, close to the maximum power point.

The shunt size naturally influenced the resulting G_{sh} parameter that increased faster than the circumference of the defect, but slower than the surface area. The resulting potential distribution in a 5 mm $\times$ 5 mm module type cell, at the maximum power point, is shown in Figure 5.9.

5.5 Modelling outlook

In parallel with the development of computers, more detailed modelling has become possible and there is no obvious reason why this development should not progress in the coming years. More memory allows for finer meshing and several processors working in parallel will speed up calculations, especially for embarrassingly parallel processes like when essentially the same calculations are carried out many times with adjustments of one or several parameters.

However, increased processing speed and memory will not necessarily solve all difficulties with simulating thin-film solar cells. The issues of handling very large aspect ratios and very small feature sizes, i.e. in the example of small defects, remain.

The 2-D device model discussed here (Section 5.3.2) does not include more advanced forms of trap distributions, tunnelling or cross-interface recombination, but it could quite readily be accommodated. This kind of features has been implemented in several of the 1-D software packages listed in Section 5.3.1. Intra-band tunnelling has been added to SCAPS in the latest version [86] and there are plans for implementations of 2-D simulations in AFORS-HET, both as a network model and as a full numerical implementation [62].

In the hybrid model, it is possible that the current distribution could be simulated using a 2-D representation of a ZAO layer instead of a thin 3-D ZAO layer, since the thin-film structure is nearly 2-D. This would increase

computation speed, allowing for the use of an inverse modelling method so that sheet resistance of the ZAO can be extracted instead of the lumped series resistance parameter used in the one diode model.

There are also software packages that are used to simulate microelectronic components. These are mostly focused on crystalline Si, but could be adapted to handle materials like the ones present in CIGS-based cells.

6. Stability

While wafer-based Si technology has a proven record of stability this issue is not quite resolved for several of the thin-film technologies, see e.g. [77, 65, 32, 71, 20, 31]. This is partly because of the relative novelty of these technologies, and partly because there are more complex processes in these devices, which are not quite understood. In order to be able to asses the influence of operational exposure during 20 years or more, a better understanding of degradation processes is needed.

6.1 Introduction to Stability Studies

From previous studies, it is quite well established that moisture in combination with high temperature has a negative influence on CIGS solar cells, as shown in Papers IV and V as well as references [89, 52, 71]. It is important to note that prolonged exposure to elevated temperature in a dry atmosphere has little influence on device performance. The degradation effects are not well understood, and different types of cell structures can be influenced differently.

The stability over time, for solar cell modules, can be divided into two levels, the inherent stability of the cells and the overall stability of the module. The overall module stability can be tackled by ensuring a strong encapsulation. To put it simply, if no moisture can find its way into the module, there will be no effect from moisture on module degradation. This can be accomplished with the right combinations of encapsulant, edge-sealing and framing. The most common methods of encapsulating wafer-based modules are not enough to protect thin-film CIGS modules, as the encapsulant of choice, EVA, readily transports water vapour. There is, of course, an intimate link between the inherent stability of the active layers and the overall module stability. While strong encapsulation can provide stable operation, long term stability may be accomplished at a lower cost if the device layers are stable in themselves, as in the case of wafer-based Si technology. The overall module stability is not studied in this work, but the subject is touched upon in connection with moisture ingress.

The inherent stability of CIGS solar cells concerns the stability of the cell structure itself, and how it reacts to degradation. This ultimately depends on the effects on the individual materials in the layers of the structure, and how these effects influence the electrical performance of the cells. The inherent stability is the chief concern of this chapter.

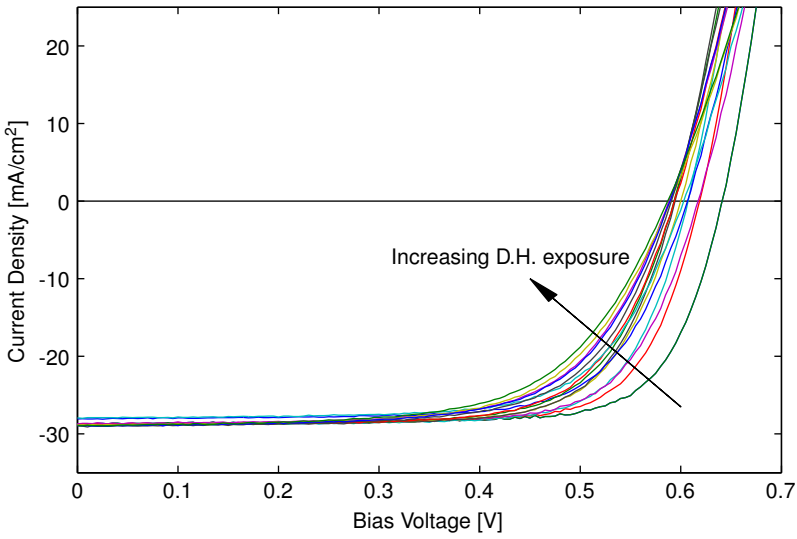

Figure 6.1: J-V curves at different stages of degradation.

6.2 Degradation of CIGS Cells

As mentioned, the most important degradation factor for CIGS solar cells is the combination of moisture and high temperature, commonly referred to as damp heat (D.H.). More specifically this is equivalent to an environment with a temperature of 85 °C and with 85 % relative humidity. It is used as an accelerated ageing test and it is defined in the design qualification and type approval standards for thin-film as well as wafer-based solar cell modules ([36] and [37], respectively).

Although D.H. exposure may influence different cells differently, and it is difficult to generalize on the degradation effects, most CIGS cells suffer from reduced V_{OC} and FF while the J_{SC} typically is not severely affected. Consequently, the η is also reduced. Initially the process is quick, but eventually saturates. This is exemplified in Figure 6.1, where *J-V* curves for increasing time of D.H. exposure are shown for a baseline cell from Ångström Solar Center. The criteria for baseline processes are given in [42].

The *J-V* curves shown here (Figure 6.1) clearly show how the performance of the cell is affected by the D.H. treatment, with the V_{OC} decrease as the most prominent feature. This is detailed in Figure 6.2a, where the evolution of the V_{OC} is plotted as a function of the exposure time. Here, it is evident that the degradation in the open circuit voltage is forceful in the beginning of the exposure time, while it subsequently saturates at a lower level.

At lower relative humidity, the typical degradation of base line cells is much less severe, without the strong initial decrease in open circuit voltage. This is studied in Paper VI, in conjunction with the effects of EVA encapsulation on

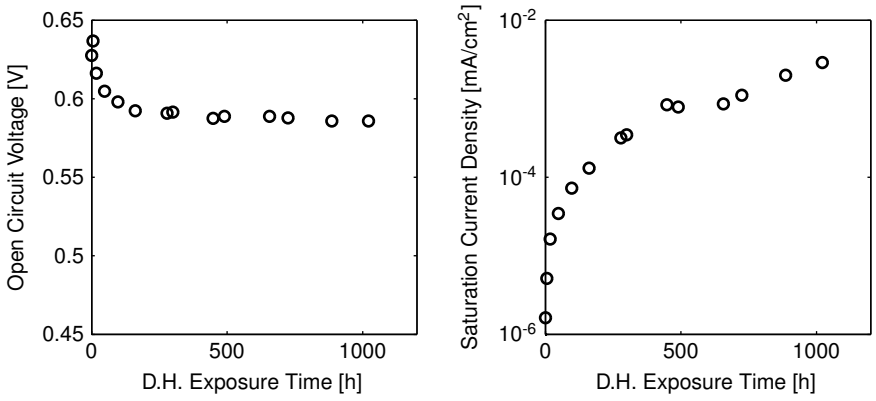

(a) V_{OC} *(b)* J_0

Figure 6.2: An example of how the open circuit voltage (a) and the saturation current density (b) develop over the course of 1000 hours of damp heat exposure. The data represent average values for four cells on the same substrate.

degradation. At 65 % relative humidity the degradation is similar to the case with 85 %, but with a longer time constant. At even lower levels the strong V_{OC} decrease is not present.

6.2.1 Degradation Mode Separation

Different degradation modes can be separated, using the parameters of the one diode model. This method can separate effects from shunt conductances, series resistances and the quality of the diode itself.

One effect that is well established is the increase of the front contact sheet resistance with exposure to D.H. [89, 47]. The back contact material that is exposed in the scribes used to isolate the different cells can be corroded in the humid environment, which also leads to increased resistance. These two resistance components influence the slope of the *J-V* curve in the forward direction, which can be seen in Figure 6.3. It is also shown clearly in the value of the ODM R_s parameter in Table 6.1.

With the effect of the series resistance separated, the degradation effects on the diode itself is quantified by the degradation of the extracted J_0 and A parameters. The development of the saturation current density is illustrated by the example in Figure 6.2b, where it is evident that the saturation current increases by several orders of magnitude, rapidly following the introduction into damp heat environment. Increased recombination is the likely process behind this development and also leads to the reduction in the open circuit voltage previously mentioned. As a consequence of the increased recombination, in

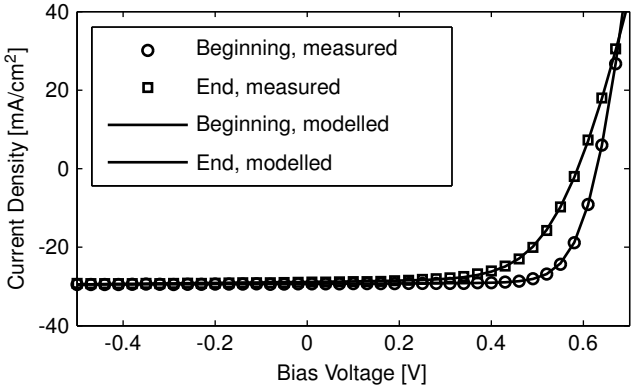

Figure 6.3: An example of illuminated *J-V* characteristics before and after 1000 h of damp heat treatment.

Table 6.1: *ODM parameters from the example of J-V characteristics before and after damp heat exposure.*

	J_0 [mA/cm^2]	A [-]	R_s [kΩcm^2]	G_{sh} [mS/cm^2]	J_L [mA/cm^2]
Before D.H.	9.3×10^{-7}	1.4	6.2×10^{-4}	0.44	29.4
After D.H.	1.4×10^{-3}	2.3	1.3×10^{-3}	1.3	28.9

combination with the increase in series resistance, the fill factor deteriorates as well.

Furthermore, the shunt conductance and the photo current can be monitored. The plots in Figure 6.3 show that these parameters do not change to a large extent, but studying the ODM parameters in Table 6.1 the G_{sh} parameter does increase significantly in relative terms, while the J_L remains essentially constant. However, this change in G_{sh} does not influence the FF or the η to a large extent.

6.2.2 Hybrid Modelling for Stability Studies

Although the extracted J_0 and A are essentially related to the quality of the diode in the solar cell, they can also be influenced by the resistivity of and the current distribution in the front contact material. This effect is described in Paper II. It is an effect of the lateral current distribution in the front contact and can be modelled using the hybrid model described in Section 5.4. Different parts of the cell experience different series resistance depending on where it is located in relation to the current collecting front contact. When added up, the *J-V* characteristics of the different parts create a distorted total *J-V* curve,

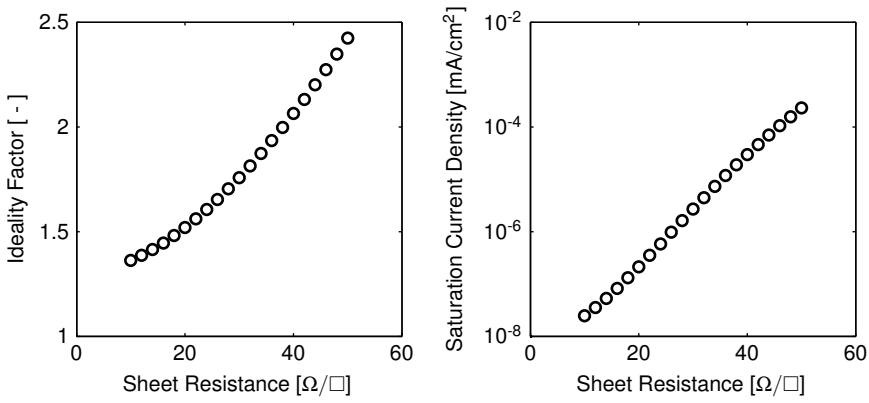

(a) *(b)*

Figure 6.4: The effects of increased ZAO sheet resistance on the extracted A (a) and J_0 (b) one diode model parameters, for module type cells.

which result in artificially high J_0 and A values when these parameters are extracted.

Although it is obvious that there are effects from the front contact sheet resistance on the extracted J_0 and A parameters, it is not enough to explain the sharp increase associated with the D.H. treatment for laboratory scale cells. With the current collecting grid used in these devices the lateral effects are small. However, for module type cells it is more difficult to separate the effects of D.H. on the diode and on the resistivity of the front contact. This is illustrated in Figure 6.4, where the extracted ideality factor and saturation current density are displayed for varying ZAO sheet resistance. In this case a 5 mm wide module type cell is used. The sheet resistance increase is in line with what can be expected from damp heat effects [45, 89]. It shows that the one diode model parameters are severely affected due to the lateral current distribution in the absence of a current collecting grid.

6.3 Absorber Thickness and Degradation

In Paper IV, the effect of the buffer layer thickness on the stability characteristics is studied. The main reason for attempting to thin down the absorber layer is that this would reduce the material consumption, which may be very important in the view of rising metal prices. The abundance of the materials used has been questioned [5, 29, 21] but is not considered a limiting factor in the CIGS community today. Furthermore, a thinner layer can be deposited faster, thus costing less in terms of machine time and investments.

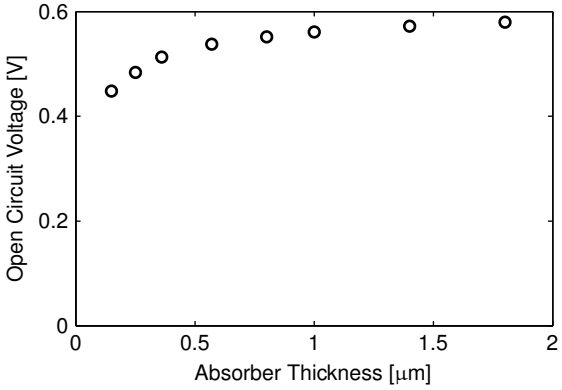

Figure 6.5: Modelled V_{OC} values as a function of the absorber thickness (calculated using AFORS-HET and the base-line case presented in Table 5.1)

In order to study the effects of D.H. on thinner absorbers, cells with varying absorber thickness between 0.36 μm and 1.8 μm were subjected to D.H. in a climate chamber. The cells with 1.8 μm absorber thickness were standard, baseline cells of the Ångström Solar Center [42]. For the other samples, only the absorber thickness was varied, while the other process steps remained within the base line specifications.

The cells with thinner absorbers differ from the base line ones in several respects. The most obvious one is that although the CIGS material has a very high absorption coefficient, some of the incoming light is absorbed at the back contact and some is reflected there, escaping through the front contact layers of the cell. This means that the generation, and thus the J_L is lower in these devices.

Furthermore, the V_{OC} is lower in the thinnest cells, more so than what can be explained as an effect of the decreased generation. This is due to increased recombination, which may be explained by the fact that the space charge region in the absorber layer extends to the back contact. A larger share of the absorber layer is taken up by the space charge region, where recombination is high due to the fact that the Fermi level lies closer to the middle of the band gap here. This effect, with decreasing V_{OC} as an effect of decreasing absorber layer thickness, is shown in Figure 6.5 for 1-D simulations made with AFORS-HET. These are based on the baseline case of Table 5.1, but with varying absorber layer thickness. That the recombination is different in the thinnest cells is also seen in $J(V)_T$ characterization, which shows evidence for interface recombination in the initial state. This may contribute to the lower initial voltage, but after the first 100 h this increased interface recombination seems to be annealed out.

Cells with an absorber thickness of 0.36 μm, 0.54 μm, 0.57 μm, 0.8 μm and 1.8 μm were exposed to damp heat treatment in a climate chamber, for a pe-

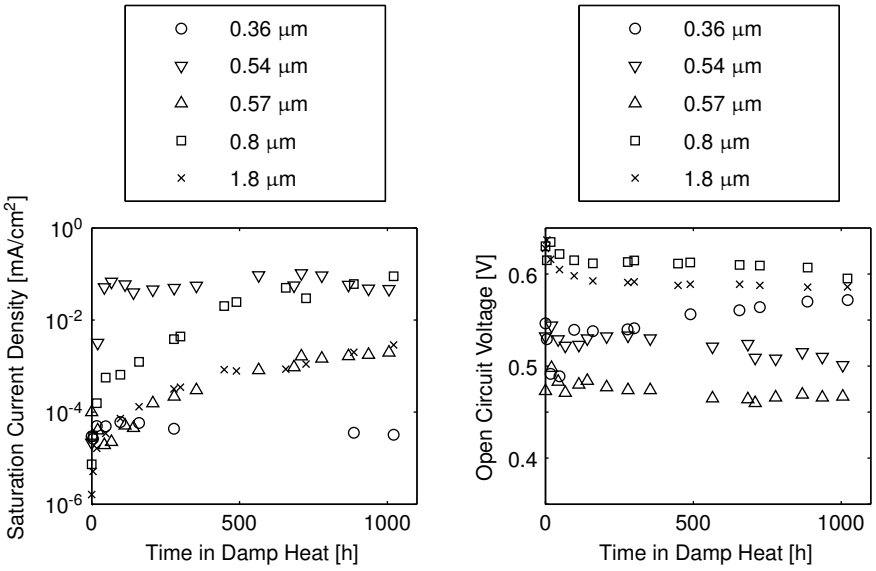

(a) *(b)*

Figure 6.6: The saturation current density (a) and the open circuit voltage (b) of cells with different absorber thicknesses.

riod of 1000 h. The cells were monitored using J-V, C-V, and $J(V)_T$ characterization. As mentioned, the main difference between the cells prior to the D.H. treatment was that the thin cells (0.36 μm to 0.57 μm) exhibited lower J_{SC} and V_{OC}, while the thinnest ones also displayed interface recombination. The cells with 0.57 μm absorber thickness had extra Na at the back contact from a precursor layer deposited prior to the CIGS evaporation.

When subjected to D.H., most of the cells were degraded much like the typical example described in Section 6.2. The development of the J_0 and the V_{OC} is shown in Figure 6.6. From Figure 6.6a it is evident that there are two exceptions that does not follow the typical pattern with a strong increase in J_0 over the D.H. exposure time. These exception are the thinnest cells (0.36 μm) and the ones with extra Na added (0.57 μm).

The thinnest cells actually increased their efficiency, open circuit voltage and fill factor during the D.H. treatment. The open circuit voltage development is shown in Figure 6.6b. Initially the V_{OC} dropped, only to return to its previous level after an exposure time of approximately 100 h. In parallel to this, J_{SC} and FF increased, indicating some sort of annealing effect at work during the first 100 h of D.H. exposure. Subsequently, the cell performance was more or less constant throughout the remainder of the 1000 h. The J_0 remained in the 10^{-5} mA/cm^2 region for the whole of the exposure.

The exact reason for this remarkable stability is difficult to pinpoint, but the fact that it only occurs in the cells where the space charge region extends to the

back contact points to the quasi neutral bulk playing a role in the degradation and that it is not related to the properties of the interface between the CIGS and the ZnO.

Compared to the reference samples with similar thickness (0.54 μm), the ones with extra Na (0.57 μm) were degraded more severely, not only in the V_{OC} but in the J_{SC} and, most prominently, in the FF. The J_0 (shown in Figure 6.6a) increases very sharply in the beginning of the treatment, while the V_{OC} displays a more normal decrease. The most likely explanation for this is that the Na precursor alters the material growth, making the resulting CIGS layer more susceptible to effects inflicted by the damp heat exposure.

6.4 Buffer Layer Material and Degradation

An issue that has attracted quite extensive research efforts in the CIGS community is that of the buffer layer. To date, CdS is the material of choice in most high efficiency laboratory cells and most manufacturing operations. However, the use of Cd may cause problems with chemical handling issues, legislation and market perceptions. Therefore, several new buffer layer materials and processes have been researched lately, in university laboratories [58, 83, 4, 75, 56] as well as at manufacturing companies [54, 50]. These materials include In_2S_3, ZnO, Zn(O,S) and (Zn,Mg)O deposited with wet chemical or vacuum methods. In Paper V, the degradation of cells with In_2S_3 and Zn(O,S) are compared to the standard CdS-buffered cells. Two types of CIGS material are also compared; one from a rate-controlled process equipment (designated BAK) and one from an equipment using end point detection process control (designated CUPRO).

These two types of absorber material differ in morhphology, texture and carrier density profile [44]. While both processes result in dense films and are able to produce quality CIGS devices, there are a number of differences. The surface roughness is higher in the CUPRO process, which leads to less interference fringes showing up in QE. This surface structure is brought about by a recrystallization in the later stages of growth [43]. From the QE spectrum it is also possible to see a difference in the long wavelength region, i.e. for photons absorbed deep down in the absorber, where the CUPRO cells display better collection. This is most likely due to a lower effective doping density, yielding a larger space charge region. While the CUPRO material typically is untextured, the BAK material is strongly (112) oriented, depending on the amount of Na present at growth [8, 9].

For the BAK CIGS, cells with the three different buffer layers were subjected to D.H. for 1000 h. In the CUPRO case, only CdS and Zn(O,S) were tested. The results from these tests show that for BAK, the degradation is quite similar for the three buffer layers, showing a strong decrease in efficiency in the beginning of the process. This is mostly due to a decrease in the V_{OC}, where the similarity between the cells with different buffer layers was even

more pronounced. This points to the conclusion that the buffer layer material is not crucial to the degradation mode.

For CUPRO material cells, the picture is quite different with the CdS-buffered cells displaying strong decrease in the V_{OC} according to the typical pattern, while for the Zn(O,S) cells the voltage initially increases and then remains constant over the 1000 h of treatment. This clearly shows that for the CUPRO material, the buffer layer does play a role in the degradation. However, it is difficult to discern what role this is, since the CUPRO/Zn(O,S) cells were plagued by low voltage in their initial state. It is probable that the processes responsible for the V_{OC} degradation in the bulk of the absorber is present in these cells as well, although it is obscured by some different mechanism pertaining to the buffer layer or the buffer–absorber interplay.

For the BAK cells the depletion region width, estimated using *C-V* characterization, did not change significantly but displayed a small increase. This change was smaller than the margin of error in the measurement. The CUPRO cells, on the other hand, displayed drastic changes of apparent depletion region width, increasing roughly by a factor three. This can be explained either as an artefact caused by charges at the absorber/buffer interface, or as a decreased effective doping concentration in the absorber material due to some change in the bulk. In either case, this indicates that the CUPRO material responds differently to the D.H. treatment, which is also seen in the fact that the choice of buffer layer is very important to the stability characteristics.

In conclusion, the degradation mode most commonly seen, with decreasing V_{OC}, originates in the bulk of the CIGS layer, in line with findings in [34]. Although this effect is present in both types of absorber materials studied, there is a difference in the reaction to D.H. and how the choice of buffer influences the degradation.

6.5 Encapsulation and Moisture Ingress

In real operation, the solar cells will be encapsulated, and with the PV encapsulation technologies at hand today it is not possible to guarantee absolute protection against moisture ingress for the full period of operation of 20 years or more. While it is possible to buy commercial systems for edge-sealing, which ensure that CIGS modules can pass the type qualification tests, it is difficult to protect the active devices completely from moisture ingress. This leads to the question of how much the solar cells are affected by heat in combination with moisture that can be suspended in the encapsulant. In Paper VI a worst case scenario is used, with the cells encapsulated using EVA but with no cover glass, allowing moisture to freely penetrate the encapsulant.

In order to evaluate the dynamics of moisture ingress into the EVA layer used as encapsulant, moisture sensors were laminated between glass and EVA and subjected to damp heat. These moisture sensors consists of two interdigitating ITO electrodes on a glass substrate, with a sensor layer of microporous TiO_2 deposited on top of them. The electrodes are patterned using

photolithography, and the TiO_2 is deposited using a doctor blading technique. This sensor structure is illustrated in Figure 6.7a.

The response of the sensor is measured using a Zahner IM6 electrochemical workstation where the frequency is swept from 100 Hz to 1 MHz. The a.c. resistance is calculated from a Nyquist plot, fitting an equivalent circuit model with a resistance and a constant phase element. Prior to usage, the sensor was calibrated in the climate chamber at different degrees of humidity within the range used in the test, and subsequently laminated. More information on the sensor can be found in [15] and [16].

In order to be able to contact cells that had been laminated, a special test structure was designed with a patterned back contact that, together with an isolation scribe, defined the cell area. This was necessary since the use of scribe lines on all sides of the cell would make contacting the front contact under the EVA layer very difficult. With the cell definition already taken care of at the back, the current collecting grid could simply be extended to the edge of the substrate, allowing for the EVA encapsulant to cover the cell completely. This test structure is shown in Figure 6.7.

When the sensors were subjected to damp heat in parallel with the test structures, it was quickly revealed that the moisture ingress into the EVA layer was very quick and saturated after a few minutes of exposure. With the long exposure times in the D.H. test, the EVA can be considered saturated with water at all times when the samples are in the climate chamber.

When laminating the cells, the V_{OC} was somewhat degraded, while the J_{SC} increased due to the anti-reflection effect of the index matching between EVA and ZnO. Subsequently, when subjected to D.H. the encapsulated cells did not exhibit as strong V_{OC} degradation as their non-encapsulated references. A decrease could be seen, but it was much less than what is typically seen in baseline cells (see Section 6.2). The most severe influence on the cells was on the isolation scribe where the Mo was exposed to the moisture in the EVA. Here corrosion was a problem that seemed to be increased by the presence of the encapsulant. The EVA alters the conditions at the surface of the device drastically. When the Mo is starting to corrode the EVA closest to the metal will be deaerated, and this can enhance the corrosion further leading to a vicious circle that swiftly leads to a breakage in the current circuit.

The conclusions that can be drawn from these experiments are that even if the encapsulant EVA is saturated with water, the degradation is reduced compared to the unprotected case. This means that the water ingress into the EVA used as an encapsulant is not a severe problem for the device in itself. However, the weakest point in a CIGS module seems to be the exposed Mo in the P3 scribe, since here the back contact material may be corroded by moisture. Mechanical scribing may also cause scratches in the Mo, which will enhance this process. Furthermore, the increase of resistivity in the ZAO will have more effect on module devices as the whole current is transported in this layer. In the test structures in Paper VI, a degraded resistivity in the ZAO layer would have had little effect on the extracted one diode model parameters, since

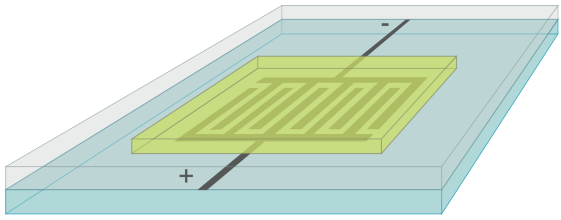

(a)

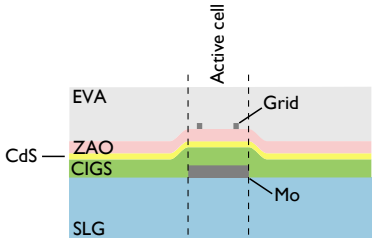

(b)

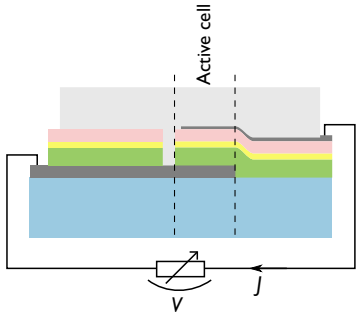

(c)

Figure 6.7: Schematics that show the moisture sensor (a) and the test structures used to evaluate effects of EVA encapsulation, (b) and (c).

they were gridded devices where the current collection did not rely on lateral conduction in the ZAO.

7. Concluding remarks

In this work, several aspects of modelling of thin-film solar cells have been investigated. Furthermore, stability of CIGS thin-film devices has been studied in accelerated ageing test using a climate chamber with controlled humidity and temperature.

Three types of modelling, analytical, numerical and hybrid methods, have been described. The analytical modelling is mostly used to gain more information from *J-V* curves than the normal solar cell parameters, and can be used in $J(V)_T$ analysis (Paper VII). Fitting the one-diode model to measurement data, information on series resistance, shunt conductance, photo current and the *p-n* junction characteristics can be extracted. This information is valuable as feed-back to process technology and for monitoring of device degradation (Papers IV, V and VI).

The hybrid modelling described here uses the one diode model to represent the *p-n* junction device, while the current distribution in the front contact is calculated numerically using the finite element method. In this way two and three dimensional effects, like device geometries, material inhomogeneities, defects and weak diode areas, may be simulated (Papers II and III). One result from using this hybrid model, is the simulation of the effects of distributed series resistance in the front contact and the effects of this on extracted one diode model parameters. With high front contact resistivity, the ideality factor and saturation current becomes artificially high. However, this problem is strongly reduced when a current collecting grid is used on the front contact.

The hybrid model is also used to study effects from material inhomogeneity and shunt defects on module type cells. From this it is evident that material inhomogeneity has little influence on the optimization of cell width and ZAO layer thickness. While the position of shunt defects on the cell is of little importance to the shunting effect, the size of the shunt naturally does play an important role. However, this effect does not scale with the circumference of the shunt or its area, but displays a more complex relationship.

While the hybrid model is useful when modelling effects from spatial inhomogeneities, it does not provide information on the inner workings of the *p-n* junction. For this purpose, numerical simulations are needed. These have been carried out in 2-D with material inhomogeneities superimposed on a homogeneous baseline case (Paper I). There, it is shown how fluctuations in parameters like the band gap and trap densities decrease the open circuit voltage of the cell.

Accelerated ageing in damp heat conditions is studied for a number of device configurations, with different absorber layer thicknesses (Paper IV), and

different buffer layer materials (Paper V). In the cells with the thinnest absorber layers, there was no degradation, but maintained performance over 1000 h of damp heat treatment. The thicker absorber cells all exhibited the degradation mode with decreased V_{OC}, which is common in CIGS cells subjected to damp heat.

With three types of buffer layer materials, CdS, In_2S_3 and Zn(O,S), the degradation pattern for one type of CIGS material was remarkably similar, showing that the buffer layer material has little influence on degradation. On the other hand, for a different CIGS material (with different deposition conditions) Zn(O,S) buffer layers displays little degradation of the V_{OC}, with CdS reference cells following the typical pattern with strong initial V_{OC} decrease and subsequent stabilization. In conclusion, the common degradation mode with decreasing V_{OC} originates in the bulk of the CIGS material, while the absorber–buffer interplay also may influence the degradation characteristics.

Devices were also subjected to damp heat when encapsulated with EVA, the normal encapsulant used in PV industry. In this study (Paper VI) the EVA was saturated with moisture, representing a worst case for a module in the field. The results showed that the V_{OC} degradation is strongly reduced in the case with EVA encapsulation. This means that the device degradation from moisture in the field should not pose a serious problem. A more important issue is the corrosion of exposed Mo, which may be enhanced by the presence of the EVA.

Summary in Swedish

Modellering av och stabilitetskaraktäristik hos CIGS-baserade tunnfilmssolceller

Solenergi har alltid varit enormt viktig för mänskligheten och har utnyttjas på många olika sätt, från att värma sig i solen till att torka kläder i vinden och odla grödor till mat. De flesta energislag har sitt ursprung i solens energi, en resurs som är enorm. Det grundläggande ämnet i den här avhandlingen är solceller som möjliggör en direkt omvandling av solenergin till elektricitet, med relativt sett hög verkningsgrad och små miljökonsekvenser.

Den teknik som solcellerna i avhandlingen behandlar baseras kring absorbatormaterialet $CuIn_{1-x}Ga_xSe_2$, som brukar förkortas CIGS. Det är ett halvledarmaterial med direkt bandgap och därmed hög absorptionskoefficient, för vilket bandgapet kan justeras genom att proportionerna mellan In och Ga ändras. CIGS-celler innehåller dessutom ett kontaktlager av Mo underst i strukturen, ett buffertskikt (oftast CdS), samt ett transparent ledande lager. Ofta utgörs detta översta skikt av ett dubbellager med tunn högohmig ZnO och aluminiumdopad ZnO (ZAO). Ovanpå detta kan en strömuppsamlande kontaktstruktur i metall deponeras.

Avhandlingen beskriver ett flertal aspekter av modellering och simulering av tunnfilmssolceller baserade på absorbatormaterialet $CuIn_{1-x}Ga_xSe_2$. Dessutom tas olika typer av elektrisk karaktärisering upp, samt studier av stabiliteten hos själva komponenterna.

Den vanligaste metoden för elektrisk karaktärisering av solceller innebär att strömmen mäts som funktion av spänning, i mörker eller under belysning, så kallad J-V-karaktärisering. Det viktigaste resultatet av dessa mätningar är solcellsparametrarna, V_{OC}, J_{SC}, FF och η, som kan utläsas från kurvan som tas upp under belysning. Mer information om cellen kan extraheras genom att en ekvivalentmodell anpassas till mätdata, vilket resulterar i ett antal modellparametrar, J_0, A, R_s, G_{sh} och J_L. Parametrarna används även för att utröna vilken rekombinationsväg som dominerar strömtransporten i cellen, utifrån J-V-mätningar vid olika temperatur. Denna analysmetod, $J(V)_T$, används i Artikel VII, där rekombination i celler med ZnO direkt på CIGS-skiktet undersöks. $J(V)_T$-analysen visar att för celler med ca 30 % Ga och direkt ZnO så domineras strömtransporten av gränsskiktsrekombination, medan för celler utan Ga så dominerar rekombination i bulken. Detta är även den normala rekombinationsmoden för celler med CGS och CdS-buffert.

Det finns ett flertal olika metoder att matematiskt modellera solceller. Ett vanligt sätt är att anpassa parametrarna i en ekvivalentmodell till mätdata, så som med endiodmodellen som beskrivs i föregående stycke. Förutom att parametrarna kan användas till att analysera rekombinationsvägar i solcellerna, så lämpar de sig till att övervaka hur cellerna försämras vid stabilitetsundersökningar. Förändringar i cellerna framträder tydligt i framförallt mättnadsströmmen.

Förutom modellering av ekvivalentkretsar analytiskt kan själva solcellen simuleras genom att Poisson's ekvation och kontinuitetsekvationerna för elektroner och hål löses. Detta ger potentialfördelningen i alla skikt, samt elektron- och håltätheter. Alternativt kan dessa ekvationer formuleras om så att kvasi-ferminivåerna används i stället för laddningsbärartätheterna som oberoende variabler. På så vis förbättras konvergensen vid lösningen. Från de beräknade storheterna och inmatade materialparametrar kan t.ex. banddiagram och strömmar beräknas.

Denna typ av simuleringar har använts i ett flertal viktiga studier av tunnfilmssolceller baserade på CIGS under de senaste 20 åren. Detta har dock i stort inskränkts till endimensionella modeller, vilka fungerar mycket väl för att undersöka hur en parameter, t.ex. ett steg i ledningsbandet mellan två lager, påverkar cellens elektriska karaktäristik. Det som däremot inte låter sig göras med en modell i en dimension är simulering av materialvariationer, korngränser, cellgeometrier, ojämnheter i gränsytor, defekter och strömuppsamlande kontaktstrukturer.

Effekter av variationer i materialparametrar simuleras här i två dimensioner. En tvådimensionell modell av ett tvärsnitt av en cell skapades i Comsol Multiphysics, med randomiserade variationer i materialparametrar överlagrade på ett basfall. I och med att bandgapet i CIGS kan justeras genom att In- och Ga-proportionerna varieras, öppnar det för variationer i bandgapet. Resultatet av simuleringarna visar hur spänningen i solcellerna minskar först måttligt och sedan allt kraftigare när standardavvikelsen för bandgapsvariationerna ökar. Samma typ av undersökningar fast med variationer i antalet fällor mitt i bandgapet ger liknande resultat med framförallt minskande spänning.

För att kunna simulera effekter av geometrier och defekter, t.ex. shuntvägar mellan fram och bakkontakten, krävs tredimensionella simuleringar. Detta är komplicerat att göra med den komponentmodell som presenterats, även om det inte finns några fundamentala skillnader mellan att använda den i två eller tre dimensioner. En mer praktiskt tillämpbar metod presenteras här, där den analytiska endiodmodellen används för att introducera solcellens *J-V*-karaktäristik som en distribuerad komponent vid gränsytan mellan buffertskiktet och ZnO-lagren. Strömtransporten i ZnO-lagren simuleras sedan numeriskt. Detta ger en hybridmodell som kan användas för att simulera makroskopiska effekter som cellgeometrier, strömuppsamling eller diskreta defekter. Metoden kan även användas för att simulera effekten av materialparametrar som varierar över cellytan. Detta beskrivs i Artikel III. Ett ytterligare användningsområde skulle kunna vara att simulera variationer i belysning, t.ex. vid koncentrerat solljus.

Den ekonomiska livslängden för en solcellsanläggning är mycket viktig för kostnaden för elen som produceras. Idag räknar man typiskt med en livslängd på 20 – 25 år, vilket är mycket rimligt för traditionella Si-moduler. Dessa har testats ingående under de senaste 30 åren, medan stabiliteten hos tunnfilmsmoduler inte har studerats lika noggrant. Även om de flesta studier pekar på att CIGS-moduler är stabila under typiska användningsförhållanden, så har det även rapporterats om att CIGS-komponenter är känsliga för en kombination av fukt och värme. I test specifikationerna för typgodkännande skall de färdiga modulerna klara av 1000 timmar i 85 °C och vid 85 % relativ luftfuktighet. När CIGS-komponenter utsätts för denna typ av behandling så minskar typiskt tomgångsspänningen snabbt under den första tiden för att sedan stabiliseras på en nivå 10 % till 20 % lägre än i utgångsläget. Parallelt med detta ökar mättnadsströmen, ofta med flera tiopotenser. Detta för även med sig en minskning av FF som förstärks av att resistiviteten i ZAO-skiktet ökar under den accelererade åldringen.

I Artiklarna IV och IV undersöks stabiliteten vid accelererad åldring av CIGS-solceller med ett antal olika variationer i strukturen. I den första studeras celler med olika tjocklek på absorbatorlagret, från normal tjocklek på 1.8 μm ned till 0.36 μm. Proverna med de tunnaste absorbatorerna uppvisar ett oväntat beteende i och med att spänningen inte minskar under behandlingen i klimatkammaren, utan istället ökar. C-V-mätningar visar att utarmningsområdet i dessa celler sträcker sig till bakkontakten, vilket inte är fallet för några av de tjockare cellerna. Detta pekar på att de processer som huvudsakligen står för försämringen sker i CIGS-skiktets bulk och inte i gränsytan mellan CIGS och buffertskikt.

Ett antal celler med tunnare absorbatorer (0.57 μm) och med extra Na deponerat före absorbatorskiktet testades också. Dessa uppvisar mycket kraftiga förändringar vid exponeringen, främst i mättnadsström och idealitetsfaktor. Troligtvis beror detta på att Na-tillskottet påverkar CIGS-materialets tillväxt så att det blir mer benäget att förändras när det utsätts för fukt och värme.

I den andra artikeln med varierande cellstrukturer studeras celler med olika buffertmaterial. I de flesta CIGS-solceller används CdS men det finns att antal olika kandidater för att ersätta detta, t.ex. In_2S_3 och Zn(O,S) som studeras i det här fallet. Dessutom studeras CdS- och Zn(O,S)-buffrade celler med två typer av CIGS-material, från två olika deponeringssystem som kallas BAK och CUPRO. Vid accelererad åldring av celler med BAK-CIGS och de tre olika buffertmaterialen uppvisar de karaktäristik som liknar varandra, med en tydlig nedgång i spänning initialt. Detta pekar på att försämringen inte sker i buffertskiktet eller i området nära gränsytan mellan CIGS och buffert.

För den andra typen av CIGS-material, som bl.a. har en annan dopningsprofil och en annan morfologi, skiljer sig dock resultatet mellan celler med CdS- och Zn(O,S)-buffrar. Medan cellerna med CdS-buffert uppvisar samma karaktäristik när det gäller V_{OC} som BAK-cellerna, så uppvisar de med CUPRO/Zn(O,S) en ökning av spänningen som sedan bibehålls under resten av behandlingen. Detta från ett utgångsläge med något lägre spänning. Samtidigt så minskar FF under tiden, vilket resulterar i minskad verkningsgrad. Slutsat-

sen här är att medan samma process i bulken bidrar till sänkning av spänningen i båda sorterna av CIGS, så döljs denna effekt av andra mekanismer i samspelet mellan CIGS och buffert när det gäller CUPRO/Zn(O,S)-komponenterna.

Acknowledgements

This work was carried out at the Division of Solid State Electronics, Department of Engineering Science, Uppsala University. I would like to acknowledge the financial support of the *Swedish Energy Agency* and *Nordic Energy Research*.

Furthermore, I would like to express my sincere thanks to the co-workers in the solar cell group. You have let me destroy your solar cells in the climate chamber and have provided a lot of input to my work over the years. Besides that, you provide a warm and amicable working environment. Special thanks to Lars and Marika for guidance and support.

Thank you FTE for a friendly working environment. And a special thanks to Marianne, a veritable rock in the stormy sea of university administrative dealings.

Jonas, you've been a perfect lunch partner for floating all sorts of ideas from how to quantify diffusion dynamics of Earl Grey tea, to how to live life in general (e.g. which "sofa-bed" to go for, or not).

Thank you Ludde, Niklas, Tobbe, Jonas ... and several others. I will not try to mention all the friends who have been invaluable to me during my university years.

A big thanks to Tupplurarna, for letting an old-timer turn up to play a few solos now and then.

Thank you Philip, Michel, Salman, Joyce, Paul, Kjell, Iain and many others for letting me escape from the solar cell world from time to time, and into your worlds of fiction.

A big thanks to all of the IEA-PVPS crowd. The Incessant Eating Agency meetings have been more than a social club to me (in spite of what it may look like from the outside). You have taught me a lot about PV in reality, and about aspects that are not so obvious from the viewpoint of the laboratory.

Thanks to the Swedish solar cell community, Mats, Jonas, Monika and many more. In order to get somewhere, the community really needs its enthusiasts.

Second to last, but certainly not least. Thank you Malin, Claes and Nils – the best family anyone could want.

And of course *Helena*, my wife. Finding you beside me every morning – what more could I wish for?

If I was a flower growing wild and free
All I'd want is you to be my sweet honey bee.

[Barry Louis Polisar]

Bibliography

[1] IEC International Standard 60904-3. Photovoltaic devices – Part 3: Measurement principles for terrestrial photovoltaic (PV) solar devices with reference spectral irradiance data. Technical report, Geneva, Switzerland, 1989.

[2] IEC International Standard 60904-8. Photovoltaic devices – Part 8: Measurement of spectral response of a photovoltaic (PV) device. Technical report, IEC, 1998.

[3] Ж. И. Алферов, В. М. Андреев, М. Б. Каган, И. И. Протасов, and В. Г. Трофим. Солнечные преобразователи на основе гетеропереходов p-$Al_xGa_{1-x}As$–n-GaAs. *Физика и техника полупроводников*, 4:2378, 1970 [Zh. I. Alferov, V. M. Andreev, M. B. Kagan, I. I. Protasov, and V. G. Trofim, Solar-energy converters based on p-n $Al_xGa_{1-x}As$-GaAs heterojunctions, *Sov. Phys. Semicond.* 4, 2047, 1971].

[4] N. A. Allsop, A. Schönmann, H.-J. Muffler, M. Bär, M. C. Lux-Steiner, and Ch.-H. Fischer. Spray-ILGAR indium sulfide buffers for $Cu(In,Ga)(S,Se)_2$ solar cells. *Progress in Photovoltaics: Research and Applications*, 13:607–616, 2005. doi:10.1002/pip.655.

[5] B.A. Andersson, C. Azar, J. Holmberg, and S. Karlsson. Material constraints for thin-film solar cells. *Energy*, 23:407–411, 1998. doi:10.1016/S0360-5442(97)00102-3.

[6] Edmond Becquerel. Mémoire sur les effets électriques produits sous l'influence des rayons solaires. *Comptes rendus hebdomadaires des séances de l'Académie des Sciences*, 9:561–567, 1839. Available from: `http://gallica.bnf.fr/ark:/12148/bpt6k2968p/f561.pagination`.

[7] J. J. M. Binsma and H. A. van der Linden. Preparation of thin cuins2 films via a two-stage process. *Thin Solid Films*, 97(3):237–243, November 1982. doi:10.1016/0040-6090(82)90458-8.

[8] Marika Bodegård, Karin Granath, and Lars Stolt. Growth of $Cu(In,Ga)Se_2$ thin films by coevaporation using alkaline precursors. *Thin Solid Films*, 361-362:9–16, February 2000. doi:10.1016/S0040-6090(99)00828-7.

[9] Marika Bodegård, Lars Stolt, and Jonas Hedström. The influence of sodium on the grain structure of $cuinse_2$ films for photovoltaic applications. In *Proceedings of the 12th European Photovoltaic Solar Energy Conference, Amsterdam*, pages 1743–1746, 1994.

[10] Kristijan Brecl and Marko Topic. Simulation of losses in thin-film silicon modules for different configurations and front contacts. *Progress in Photovoltaics: Research and Applications*, 16(6):479–488, 2008. doi:10.1002/pip.831.

[11] M. Burgelman and A. Niemegeers. Calculation of CIS and CdTe module efficiencies. *Solar Energy Materials and Solar Cells*, 51(2):129–143, February 1998. doi:10.1016/S0927-0248(97)00227-4.

[12] Marc Burgelman, Johan Verschraegen, Stefaan Degrave, and Peter Nollet. Modeling thin-film PV devices. *Progress in Photovoltaics: Research and Applications*, 12:143–153, 2004. doi:10.1002/pip.524.

[13] Marc Burgelman, Alex De Vos, and Alex Niemegeers. Device simulation of polycrystalline heterojunction solar cells. In *Proceedings of the 12th European Photovoltaic Solar Energy Conference, Amsterdam*, pages 1557–1560, 1994.

[14] A.R. Burgers, J.A. Eikelboom, A. Schönecker, and W.C. Sinke. Improved Treatment of the Strongly Varying Slope in Fitting Solar Cell I–V Curves. In *Conference Record of the Twenty Fifth IEEE Photovoltaic Specialists Conference*, pages 569–572, 1996. doi:10.1109/PVSC.1996.564070.

[15] Thomas Carlsson, Janne Halme, Peter Lund, and Petri Konttinen. Moisture sensor at glass/polymer interface for monitoring of photovoltaic module encapsulants. *Sensors and Actuators A: Physical*, 125(2):281–287, January 2006. doi:10.1016/j.sna.2005.07.022.

[16] Thomas Carlsson, Petri Konttinen, Ulf Malm, and Peter Lund. Absorption and desorption of water in glass/ethylene-vinyl-acetate/glass laminates. *Polymer Testing*, 25:615–622, 2006. doi:10.1016/j.polymertesting.2006.04.006.

[17] D. M. Chapin, C. S. Fuller, and G. L. Pearson. A new silicon p-n junction photocell for converting solar radiation into electrical power. *Journal of Applied Physics*, 25(5):676–677, 1954. doi:10.1063/1.1721711.

[18] J. David Cohen, Jennifer T. Heath, and William Shafarman. New Junction Capacitance Methods for the Study of Defect Distribution and Carrier Properties in the Copper Indium Diselenide Alloys. In *Mat.Res.Soc.Symp.Proc. Vol. 763*, pages B9.1.1–B9.1.12, 2003.

[19] Michal Cwil, Małgorzata Igalson, Paweł Zabierowski, and Susanne Siebentritt. Charge and doping distributions by capacitance profiling in $Cu(In,Ga)Se_2$ solar cells. *Journal of Applied Physics*, 103(6):063701, 2008. doi:10.1063/1.2884708.

[20] Kevin D. Dobson, Iris Visoly-Fisher, Gary Hodes, and David Cahen. Stability of cdte/cds thin-film solar cells. *Solar Energy Materials and Solar Cells*, 62(3):295–325, May 2000. doi:10.1016/S0927-0248(00)00014-3.

[21] Andrea Feltrin and Alex Freundlich. Material considerations for terawatt level deployment of photovoltaics. *Renewable Energy*, 33(2):180–185, February 2008. doi:10.1016/j.renene.2007.05.024.

[22] S.J. Fonash. Analysis of Microelectronic and Photonic Structures (AMPS) software was developed at Pennsylvania State University under the direction of S.J. Fonash with funding from the Electric Power Research Institute. Available from: `http://www.cneu.psu.edu/amps/`.

[23] A. Froitzheim, R. Stangl, L. Elstner, M. Kriegel, and W. Fuhs. AFORS-HET: A computer-program for the simulation of hetero-junction solar cells to be distributed for public use. In *Proceddings of the 3rd World Conference on Photovoltaic Energy Conversion*, 2003.

[24] Andrew M. Gabor, John R. Tuttle, Michael H. Bode, Amy Franz, Andrew L. Tennant, Miguel A. Contreras, Rommel Noufi, D. Garth Jensen, and Allen M. Hermann. Band-gap engineering in Cu(In,Ga) Se_2 thin films grown from $(In,Ga)_2Se_3$ precursors. *Solar Energy Materials and Solar Cells*, 41-42:247–260, June 1996. doi:10.1016/0927-0248(95)00122-0.

[25] M. Gloeckler, A.L. Fahrenbruch, and J.R. Sites. Numerical modeling of CIGS and CdTe solar cells: setting the baseline. In *Proceedings of 3rd World Conference on Photovoltaic Energy Conversion*, pages 491–494, 2003.

[26] M. Gloeckler and J.R. Sites. Efficiency limitations for wide-band-gap chalcopyrite solar cells. *Thin Solid Films*, 480-481:241–245, June 2005. doi:10.1016/j.tsf.2004.11.018.

[27] P.O. Grabitz, U. Rau, and J.H. Werner. Modeling of spatially inhomogeneous solar cells by a multi-diode approach. *Physica Status Solidi (a)*, 202:2920–2927, 2005. doi:10.1002/pssa.200521205.

[28] Martin A. Green. *Solar Cells: Operating Principles, Technology, and System Applications*. Prentice Hall, 1982.

[29] Martin A. Green. Improved estimates for Te and Se availability from Cu anode slimes and recent price trends. *Progress in Photovoltaics: Research and Applications*, 14(8):743–751, 2006. doi:10.1002/pip.703.

[30] L. Gütay and G.H. Bauer. Lateral variations of optoelectronic quality of $Cu(In_{1-x}Ga_x)Se_2$ in the submicron-scale. *Thin Solid Films*, 487(1-2):8–13, September 2005. doi:10.1016/j.tsf.2005.01.026.

[31] J. F. Guillemoles. The puzzle of Cu(In,Ga)Se_2 (CIGS) solar cells stability. *Thin Solid Films*, 403–404:405–409, 2002. doi:10.1016/S0040-6090(01)01519-X.

[32] J.-F. Guillemoles, L. Kronik, D. Cahen, U. Rau, A. Jasenek, and H.-W. Schock. Stability Issues of Cu(In,Ga)Se_2-Based Solar Cells. *Journal of Physical Chemistry B*, 104(20):4849–4862, 2000. doi:10.1021/jp993143k.

[33] W. Hoffmann and M. Viaud. Competitiveness of Grid-Connected PV Solar Electricity Without Support and Its Impact on Off-Grid 3rd World Applications. In *20th European Photovoltaic Solar Energy Conference*, pages 2873–2878, 2005.

[34] M. Igalson, M. Wimbor, and J. Wennerberg. The change of the electronic properties of CIGS devices induced by the 'damp heat' treatment. *Thin Solid Films*, 403–404:320–324, 2002. doi:10.1016/S0040-6090(01)01510-3.

[35] M. Igalson and P. Zabierowski. Transient capacitance spectroscopy of defect levels in CIGS devices. *Thin Solid Films*, 361–362:371–377, 2000. doi:10.1016/S0040-6090(99)00822-6.

[36] International Electrotechnical Commission. IEC 61646 Thin-film terrestrial photovoltaic (PV) modules Design qualification and type approval. Technical report, Geneva, Switzerland, 1996.

[37] International Electrotechnical Commission. IEC 61215 Crystalline Silicon Terrestrial Photovoltaic (PV) Modules - Design Qualification and Type Approval. Technical report, Geneva, Switzerland, 2005.

[38] Joar Johansson, Uwe Zimmermann, and Marika Edoff. Modelling adnd optimization of CIGS modules. In *Proceedings of the 22nd European Photovoltaic Solar Energy Conference*, pages 1922 – 1925, 2007.

[39] Vijay K. Kapur, Ashish Bansal, Phucan Le, and Omar I. Asensio. Non-vacuum processing of $CuIn_{1-x}Ga_xSe_2$ solar cells on rigid and flexible substrates using nanoparticle precursor inks. *Thin Solid Films*, 431-432:53–57, May 2003. doi:10.1016/S0040-6090(03)00253-0.

[40] V. G. Karpov, A. D. Compaan, and Diana Shvydka. Effects of nonuniformity in thin-film photovoltaics. *Applied Physics Letters*, 80(22):4256–4258, 2002. doi:10.1063/1.1483118.

[41] L. L. Kerr, Sheng S. Li, S. W. Johnston, T. J. Anderson, O. D. Crisalle, W. K. Kim, J. Abushama, and R. N. Noufi. Investigation of defect properties in cu(in,ga)se2 solar cells by deep-level transient spectroscopy. *Solid-State Electronics*, 48(9):1579–1586, September 2004. doi:10.1016/j.sse.2004.03.005.

[42] J. Kessler, M. Bodegård, J. Hedström, and L. Stolt. Baseline Cu(In,Ga)Se_2 device production: Control and statistical significance. *Solar Energy Materials & Solar Cells*, 67:67–76, 2001. doi:10.1016/S0927-0248(00)00264-6.

[43] J. Kessler, C. Chityuttakan, J. Lu, J. Schöldström, and L. Stolt. Cu(In,Ga)Se_2 thin films grown with a Cu-poor/rich/poor sequence: growth model and structural considerations. *Progress in Photovoltaics: Research and Applications*, 11:319–331, 2003. doi:10.1002/pip.495.

[44] J. Kessler, C. Chityuttakan, J. Schöldström, and L. Stolt. Growth of Cu(In,Ga)Se_2 films using a Cu-poor/rich/poor sequence: substrate temperature effects. *Thin Solid Films*, 431–432:1–5, 2003. doi:10.1016/S0040-6090(03)00222-0.

[45] Joachim Klaer, Roland Scheer, Reiner Klenk, Axel Boden, and Christine Köble. Stress behaviour of $CuInS_2$ thin film PV-modules studied by a specific test structure. In *Proceedings of the 19th European Photovoltaic Solar Energy Conference*, pages 1847–1850, 2004.

[46] Reiner Klenk. Characterisation and modelling of chalcopyrite solar cells. *Thin Solid Films*, 387:135–140, 2001. doi:10.1016/S0040-6090(00)01736-3.

[47] Oliver Kluth, Gunnar Schöpe, Bernd Rech, Richard Menner, Mike Oertel, Kay Orgassa, and Hans Werner Schock. Comparative material study on RF and DC magnetron sputtered ZnO:Al films. *Thin Solid Films*, 502(1-2):311–316, April 2006. doi:10.1016/j.tsf.2005.07.313.

[48] Takeshi Kojima, Tadamasa Koyanagi, Kuniomi Nakamura, Takeshi Yanagisawa, Kiyoshi Takahisa, Mikihiko Nishitani, and Takahiro Wada. Stability of Cu(In,Ga)Se_2 solar cells and evaluation by C-V characteristics. *Solar Energy Materials and Solar Cells*, 50:87–95, 1998. doi:10.1016/S0927-0248(97)00126-8.

[49] Kosuke Kurokawa, Keiichi Komoto, Peter van der Vleuten, and David Faiman. *Energy from the Desert*. Earthscan, September 2006.

[50] Katsumi Kushiya, Muneyori Tachiyuki, Yoshinori Nagoya, Atsushi Fujimaki, Baosheng Sang, Daisuke Okumura, Masao Satoh, and Osamu Yamase. Progress in large-area Cu(InGa)Se_2-based thin-film modules with a Zn(O,S,OH)$_x$ buffer layer. *Solar Energy Materials and Solar Cells*, 67(1-4):11–20, March 2001. doi:10.1016/S0927-0248(00)00258-0.

[51] Jonas Malmström. *On Generation and Recombination in Cu(In,Ga)Se_2 Thin-Film Solar Cells*. PhD thesis, Uppsala University, 2005. Available from: `http://www.diva-portal.org/diva/getDocument?urn_nbn_se_uu_diva-5721-1__fulltext.pdf`.

[52] Jonas Malmström, Johan Wennerberg, and Lars Stolt. A study of the influence of the Ga content on the long-term stability of Cu(In,Ga)Se_2 thin film solar cells. *Thin Solid Films*, 431–432:436–442, 2003. doi:10.1016/S0040-6090(03)00185-8.

[53] G. Marland, T.A. Boden, and R. J. Andres. Global, Regional, and National CO_2 Emissions. In Trends: A Compendium of Data on Global Change. Technical report, Carbon Dioxide Information Analysis Center, Oak Ridge National Laboratory, Oak Ridge, Tenn., U.S.A., 2007. Available from: `http://cdiac.ornl.gov/trends/trends.htm`.

[54] Kentaro Matsunaga, Takashi Komaru, Yuji Nakayama, Tomoyuki Kume, and Yasuhiro Suzuki. Mass-Production Technology for CIGS Modules. In *Technical Digest of the International PVSEC-17, Fukuoka, Japan*, pages 455–457, 2007.

[55] Takashi Minemoto, Takuya Matsui, Hideyuki Takakura, Yoshihiro Hamakawa, Takayuki Negami, Yasuhiro Hashimoto, Takeshi Uenoyama, and Masatoshi Kitagawa. Theoretical analysis of the effect of conduction band offset of window/CIS layers on performance of CIS solar cells using device simulation. *Solar Energy Materials and Solar Cells*, 67(1-4):83–88, March 2001. doi:10.1016/S0927-0248(00)00266-X.

[56] Tokio Nakada and Masayuki Mizutani. 18% efficiency Cd-free Cu(In,Ga)Se_2 thin-film solar cells fabricated using chemical bath deposition (CBD)-ZnS buffer layers. *Japanese Journal of Applied Physics, Part 2: Letters*, 41:L165–L167, 2002. doi:10.1143/JJAP.41.L165.

[57] A. Niemegeers, M. Burgelman, R. Herberholz, U. Rau, D. Hariskos, and H.-W. Schock. Model for electronic transport in Cu(In,Ga)Se_2 solar cells. *Progress in Photovoltaics: Research and Applications*, 6:407–421, 1998. doi:10.1002/(SICI)1099-159X(199811/12)6:6<407::AID-PIP230>3.0.CO;2-U.

[58] C. Platzer-Björkman, T. Törndahl, D. Abou-Ras, J. Malmström, J. Kessler, and L. Stolt. Zn(O,S) buffer layers by atomic layer deposition in Cu(In,Ga)Se_2 based thin film solar cells: Band alignment and sulfur gradient. *Journal of Applied Physics*, 100(4):044506, 2006. doi:10.1063/1.2222067.

[59] M. Powalla and B. Dimmler. Scaling up issues of CIGS solar cells. *Thin Solid Films*, 361-362:540–546, February 2000. doi:10.1016/S0040-6090(99)00849-4.

[60] Giora Proskurowski, Marvin D. Lilley, Jeffery S. Seewald, Gretchen L. Früh-Green, Eric J. Olson, John E. Lupton, Sean P. Sylva, and Deborah S. Kelley. Abiogenic Hydrocarbon Production at Lost City Hydrothermal Field. *Science*, 319:604 – 607, 2008. doi:10.1126/science.1151194.

[61] D. Pysch, A. Mette, and S.W. Glunz. A review and comparison of different methods to determine the series resistance of solar cells. *Solar Energy Materials and Solar Cells*, 91(18):1698–1706, November 2007. doi:10.1016/j.solmat.2007.05.026.

[62] Stangl R, Geipel T, Dubiel M, Kriegel M, El-Shater T, and Lips K. AFORS-HET 3.0: First Approach to a Two Dimensional Simulation of Solar Cells. In *Proceedings of the 22nd European Photovoltaic Solar Energy Conference*, pages 82–86, 2007.

[63] U. Rau. Tunneling-enhanced recombination in Cu(In, Ga)Se_2 heterojunction solar cells. *Applied Physics Letters*, 74:111–113, 1999. doi:10.1063/1.122967.

[64] U. Rau, P. O. Grabitz, and J. H. Werner. Resistive limitations to spatially inhomogeneous electronic losses in solar cells. *Applied Physics Letters*, 85:6010–6012, 2004. doi:10.1063/1.1835536.

[65] Uwe Rau, Axel Jasenek, Rainer Herberholz, Hans-Werner Schock, Jean-Francois Guillemoles, Daniel Lincot, and Leeor Kronik. The Inherent Stability of Cu(In,Ga)Se_2-Based Solar Cells. In *2nd World Conference and Exhibition on Photovoltaic Solar Energy Conversion*, pages 428–433, 1998.

[66] Uwe Rau and Hans W. Schock. *Clean Electricity From Photovoltaics*, chapter 7. Imperial College Press, 2001.

[67] J.J. Rembold, T.W. Curtis, J.T. Heath, D.L. Young, S.W. Johnston, and W.N. Shafarman. Electronic defects and device performance in $CuGaSe_2$ solar cells. In *Proceedings Materials Research Society Symposium. Volume 1012. Thin-Film Compound Semiconductor Photovoltaics*, pages 425–430, 2007.

[68] C. Rincón and J. González. Temperature Dependence of the Bandgap in $CuInSe_2$. *Solar Cells*, 16:357–362, 1986. doi:10.1016/0379-6787(86)90095-5.

[69] M. R. Schmer, K. P. Vogel, R. B. Mitchell, and R. K. Perrin. Net energy of cellulosic ethanol from switchgrass. *PNAS*, 105:464–469, 2007. doi:10.1073/pnas.0704767105.

[70] Dieter Schmid, Martin Ruckh, and Hans Werner Schock. A comprehensive characterization of the interface in Mo/CIS/CdS/ZnO solar cells structure. *Solar Energy Materials and Solar Cells*, 41:281–294, 1996. doi:10.1016/0927-0248(95)00107-7.

[71] M. Schmidt, D. Braunger, R. Schäffler, H.W. Schock, and U. Rau. Influence of damp heat on the electrical properties of Cu(In,Ga)Se_2 solar cells. *Thin Solid Films*, 361–362:283–287, 2000. doi:10.1016/S0040-6090(99)00820-2.

[72] Ruud E.I. Schropp and Miro Zeman. *Amorphous and microcrystalline silicon solar cells: modeling, materials and device technology*. Kluwer Academic, 1998. http://libris.kb.se/bib/5659897.

[73] John H. Scofield, A. Duda, D. Albin, B. L. Ballard, and P. K. Predecki. Sputtered molybdenum bilayer back contact for copper indium diselenide-based polycrystalline thin-film solar cells. *Thin Solid Films*, 260(1):26–31, May 1995. doi:10.1016/0040-6090(94)06462-8.

[74] Jiyon Song, Sheng S. Li, C. H. Huang, O. D. Crisalle, and T. J. Anderson. Device modeling and simulation of the performance of Cu(In_{1-x},Ga_x)Se_2 solar cells. *Solid-State Electronics*, 48:73–79, 2004. doi:10.1016/S0038-1101(03)00289-2.

[75] S. Spiering, D. Hariskos, M. Powalla, N. Naghavi, and D. Lincot. Cd-free Cu(In,Ga)Se_2 thin-film solar modules with In_2S_3 buffer layer by ALCVD. *Thin Solid Films*, 431–432:359–363, 2003. doi:10.1016/S0040-6090(03)00151-2.

[76] S. Spiering, D. Hariskos, S. Schroder, and M. Powalla. Stability behaviour of Cd-free Cu(In,Ga)Se_2 solar modules with In_2S_3 buffer layer prepared by atomic layer deposition. *Thin Solid Films*, 480–481:195–198, June 2005. doi:10.1016/j.tsf.2004.11.056.

[77] D. L. Staebler and C. R. Wronski. Reversible conductivity changes in discharge-produced amorphous Si. *Thin Solid Films*, 31:292–294, 1977. doi:10.1063/1.89674.

[78] S.M. Sze. *Physics of Semiconductor Devices*. John Wiley & Sons, 2nd edition, 1981.

[79] Task 1 - Information exchange and dissemination. Trends in photovoltaic applications. survey report of selected iea countries between 1992 and 2006. Technical report, IEA PVPS, 2007. Available from: `http://www.iea-pvps.org/products/download/rep1_16.pdf`.

[80] M. Topic, F. Smole, and J. Furlan. Computer model for simulation of amorphous silicon solar cell structures. In *7th Mediterranean Electrotechnical Conference. Proceedings (Cat. No.94CH3388-6)*, volume vol.2, pages 621–4, Antalya, Turkey, 1994. IEEE. doi:10.1109/MELCON.1994.381014.

[81] M. Topic, F. Smole, and J. Furlan. Examination of blocking current-voltage behaviour through defect chalcopyrite layer in ZnO/CdS/Cu(In,Ga)Se_2/Mo solar cell. *Solar Energy Materials and Solar Cells*, 49(1-4):311–317, December 1997. doi:10.1016/S0927-0248(97)00058-5.

[82] Marko Topic, Franc Smole, and Joze Furlan. Band-gap engineering in CdS/Cu(In,Ga)Se_2 solar cells. *Journal of Applied Physics*, 79:8537–8540, 1996. doi:10.1063/1.362533.

[83] T. Törndahl, C. Platzer-Björkman, J. Kessler, and M. Edoff. Atomic layer deposition of $Zn_{1-x}Mg_xO$ buffer layers for Cu(In,Ga)Se_2 solar cells. *Progress in Photovoltaics: Research and Applications*, 15(3):225–235, 2007. doi:10.1002/pip.733.

[84] J. R. Tuttle, J.R. Sites, A. Delahoy, W. Shafarman, B. Basol, S. Fonash, J. Gray, R. Menner, J. Phillips, A. Rockett, J. Scofield, F. R. Shapiro, P. Singh, V. Suntharalingam, D. Tarrant, T. Walter, S. Wiedeman, and T. M. Peterson. Characterization and Modeling of Cu(In,Ga)(S,$Se)_2$-based Photovoltaic Devices: A Laboratory and Industrial Perspective. *Progress in Photovoltaics*, 3:89–104, 1995. doi:10.1002/pip.4670030202.

[85] John R Tuttle, T.A. Berens, J. Keane, K.R. Ramanathan, J. Granata, R.N. Bhattacharya, H. Wiesner, M.A. Contreras, and R. Noufi. Investigations into alternative substrate, absorber, and buffer layer processing for Cu(In,Ga)Se_2-based solar cells. In *Conference Record of the IEEE Photovoltaic Specialists Conference*, pages 797–800, 1996. doi:10.1109/PVSC.1996.564248.

[86] J. Verschraegen and M. Burgelman. Numerical modeling of intra-band tunneling for heterojunction solar cells in scaps. *Thin Solid Films*, 515(15):6276–6279, May 2007. doi:10.1016/j.tsf.2006.12.049.

[87] M.B. von der Linden, R.E.I. Schropp, W.G.J.H.M. van Sark, M. Zeman, G. Tao, and J.W. Metselaar. The influence of tco texture on the spectral response of a-si:h solar cell. In *Proceedings of the 11th European Photovoltaic Solar Energy Conference*, pages 647–650, 1992.

[88] T. Wada, N. Kohara, S. Nishiwaki, and T. Negami. Characterization of the Cu(In,Ga)Se_2/Mo interface in CIGS solar cells. *Thin Solid Films*, 387(1-2):118–122, May 2001. doi:10.1016/S0040-6090(00)01846-0.

[89] J. Wennerberg, J. Kessler, M. Bodegård, and L. Stolt. Damp heat testing of high performance CIGS thin film solar cells . In *2nd World Conference and Exhibition on Photovoltaic Solar Energy Conversion*, pages 1161–1164, 1998.

[90] P.-O. Westin, U. Zimmermann, and M. Edoff. Laser patterning of P2 interconnect via in thin-film CIGS PV modules. *Solar Energy Materials and Solar Cells*, 92(10):1230–1235, October 2008. doi:10.1016/j.solmat.2008.04.015.

[91] Akimasa Yamada, Koji Matsubara, Keiichiro Sakurai, Shogo Ishizuka, Hitoshi Tampo, Paul J. Fons, Kakuya Iwata, and Shigeru Niki. Effect of band offset on the open circuit voltage of heterojunction $CuIn_{1-x}Ga_xSe_2$ solar cells. *Applied Physics Letters*, 85(23):5607–5609, 2004. doi:10.1063/1.1831566.

[92] Takeshi Yanagisawa and Takeshi Kojima. The stability of the $CuInSe_2$ solar mini-module I-V characteristics under continuous and light/dark irradiation cycle tests. *Microelectronics Reliability*, 43:503–507, 2003. doi:10.1016/S0026-2714(02)00349-9.

[93] M. Zeman, J.A. Willemen, S. Solntsev, and J.W. Metselaar. Extraction of amorphous silicon solar cell parameters by inverse modelling. *Solar Energy Materials and Solar Cells*, 34(1-4):557–563, September 1994. doi:10.1016/0927-0248(94)90085-X.

[94] Uwe Zimmermann, Marta Ruth, and Marika Edoff. Cadmium-free CIGS mini-modules with ALD-grown Zn(O,S)-based buffer layers. In *Proceedings of the 21st European Photovoltaic Solar Energy Conference*, pages 1831–1834, 2006.

Acta Universitatis Upsaliensis

Digital Comprehensive Summaries of Uppsala Dissertations from the Faculty of Science and Technology 554

Editor: The Dean of the Faculty of Science and Technology

A doctoral dissertation from the Faculty of Science and Technology, Uppsala University, is usually a summary of a number of papers. A few copies of the complete dissertation are kept at major Swedish research libraries, while the summary alone is distributed internationally through the series Digital Comprehensive Summaries of Uppsala Dissertations from the Faculty of Science and Technology. (Prior to January, 2005, the series was published under the title "Comprehensive Summaries of Uppsala Dissertations from the Faculty of Science and Technology".)

Distribution: publications.uu.se
urn:nbn:se:uu:diva-9291

ACTA
UNIVERSITATIS
UPSALIENSIS
UPPSALA
2008